Thermo Electron Co. (Waltham, MA, USA). Leflunomide, A771726, gefitinib, imatinib, amiodarone, methotrexate, L-hydroxyproline, azophloxin and aniline blue were from Wako Pure Chemicals (Tokyo, Japan). Xylidine ponceau was from WALDECK GmbH and Co. (Muenster, Germany), and Mayer's hematoxylin, 1% eosin alcohol solution, mounting medium for histological examination (malinol) and Weigert's iron hematoxylin were purchased from MUTO Pure Chemicals (Tokyo, Japan). 4,6-Diamino-2-phenylindole (DAPI) was from Dojindo (Kumamoto, Japan). ELISA kits for CTGF were obtained from Pepro Tech Inc. (Rocky Hill, NJ, USA). A771726 derivatives (compounds 1, 2 and 3) were synthesized as described previously.[29] Male C57BL/6 wild-type mice (6–8 weeks old) were used throughout the study. Male Wistar rats (6–8 weeks of age) were obtained from Kyudoh Co. (Kumamoto, Japan). The experiments and procedures described in this study were carried out in accordance with the Guide for the Care and Use of Laboratory Animals as adopted and promulgated by the National Institutes of Health, and were approved by the Animal Care Committee of Kumamoto University.

Cell culture and immunostaining. A549 cells were cultured in DMEM medium supplemented with 10% FBS, 100 Units/ml penicillin and 100 μg/ml streptomycin in a humidified atmosphere of 95% air with 5% CO_2 at 37°C.

For immunostaining, A549 cells were grown in the Lab-Tek II chamber slide system (Nalge Nunc International, Rochester, NY, USA). Cells were fixed in ice-cold acetone for 20 min, blocked with goat serum for 15 min and then incubated for 12 h with antibody against E-cadherin or α-SMA in the presence of 2.5% bovine serum albumin (BSA), before finally being incubated for 3 h with Alexa Fluor 488 goat anti-mouse IgG. Samples were mounted with VECTASHIELD. Images were captured on a confocal laser-scanning fluorescence microscope (FLUOVIEW FV500-IX-UV, Olympus, Tokyo, Japan).

Primary cultured alveolar epithelial cells were prepared from the lungs of adult pathogen-free male Wistar rats, as described previously.[39,40] Briefly, trypsin was used to dissociate the cells from the lung tissues. The resultant cell suspension was incubated on petri dishes for 60 min to remove other types of cells. Cells were suspended in DMEM and cultured for 24 h to remove nonadherent cells. The purity of the type II cells was ~95%, as described previously.[39]

Real-time RT-PCR analysis. Real-time RT-PCR was performed as described previously,[41] with some modifications. Total RNA was extracted from pulmonary tissues using an RNeasy kit, according to the manufacturer's protocol. Samples (2.5 μg RNA) were reverse transcribed using a first-strand cDNA synthesis kit. Synthesized cDNA was used in real-time RT-PCR (Chromo 4 instrument; Bio-Rad Laboratories) experiments using iQ SYBR GREEN Supermix, and analyzed with Opticon Monitor Software (Tokyo, Japan). Specificity was confirmed by electrophoretic analysis of the reaction products and by the inclusion of template- or reverse transcriptase-free controls. To normalize the amount of total RNA present in each reaction, *actin* cDNA was used as an internal standard.

Primers were designed using the Primer3 website. The primers used were (name: forward primer, reverse primer): For humans, *α-sma*: 5′-CATCATGCGTCTGGATCTGG-3′, 5′-GGACAATCTCACGCTCAGCA-3′; *tgf-β1*: 5′-AAGGACCTCGGCTGGAAGTG-3′, 5′-CCGGGTTATGCTGGTTGTA-3′; *twist*: 5′-GTCCGCAGTCTTACGAGGAG-3′, 5′-TGAATCTTGCTCAGCTTGTCC-3′; *snail*: 5′-GCCTAGCGAGTGGTTCTTCT-3′, 5′-TAGGGCTGCTGGAAGGTAAA-3′; *slug*: 5′-GAGCATTTGCAGACAGGTCA-3′, 5′-ACAGCAGCCAGATTCCTCAT-3′; *sip1*: 5′-TACGGATCCCGAAACGATAC-3′, 5′-CCTCGTGGTCTGATTTGGTT-3′; *dhodh*: 5′-ACATTGCCAGTGTGGTCAAA-3′, 5′-TCAGCCCTCCTGTTTCAGAG-3′; *timp-1*: 5′-TGACATCCGGTTCGTCTACA-3′, 5′-TGCAGTTTTCCAGCAATGAG-3′; *mmp-2*: 5′-AGTCTGAAGAGCGTGAAG-3′, 5′-CCAGGTAGGAGTGAGAATG-3′; *mmp-9*: 5′-TGACAGCGACAAGAAGTG-3′, 5′-CAGTGAAGCGGTACATAGG-3′; *notch-1*: 5′-CAGCACCTTGGCGGTCTCGTA-3′, 5′-CAATGTGGATGCCGCAGTTGTG-3′; *notch-2*: 5′-CAGGGGGCACTGACAGTAAT-3′, 5′-GGAATGCAAGTGCAGAGTGG-3′; *notch-3*: 5′-AGATTCTCATCCGAAACCGCTCTA-3′, 5′-GGGGTCTCCTCCTTGCTATCCTG-3′; *notch-4*: 5′-GCGGAGGCAGGGTCTCAACGGATG-3′, 5′-AGGAGGCGGGATCGGAATGT-3′; *jagged-1*: 5′-CGGGATTTGGTTAATGGTTATC-3′, 5′-ATAGTCACTGGCACGGTTGTAGCAC-3′; *dll-1*: 5′-GGAATGCAAGTGCAGAGTGG-3′, 5′-TCTTGCAGGGCTTATGGTGT-3′; *E-cadherin*: 5′-TGCCCAGAAAATGAAAAAGG-3′, 5′-GTGTATGTGGCAATGCGTTC-3′; *col1a1*: 5′-CCCTGTCTGCTTCCTGTAAACT-3′, 5′-CATGTTCGGTTGGTCAAAGATA-3′; *actin*: 5′-GGACTTCGAGCAAGAGATGG-3′, 5′-AGCACTGTGTTGGCGTACAG-3′. For rat; *sip1*: 5′-TACGGATCCCGAGACGATAC-3′, 5′-CCTCGTGGTCTGATTTGGTT-3′; *notch-1*: 5′-CTCACGCTGATGTCAATGCT-3′, 5′-CGTTCTTCAGGAGCACAACA-3′; *jagged-1*: 5′-GCGCACTGTGAGAACAACAT-3′, 5′-GTTTTCCCTTTCCACCCATT-3′; *col1a1*: 5′-ATGTCGCTATCCAGCTGACC-3′, 5′-TTGAGGTTGCCAGTCTGTTG-3′; *e-cadherin*: 5′-ATCTCCCTGGAAGCAGGATT-3′, 5′-CGGGCTTTGCTGGTGATG-3′; *α-sma*: 5′-GGTCAGGATCCCTCTCTTGCT-3′, 5′-CATGTTCGGTTGGTCAAAGATA-3′; *gapdh*: 5′-ATGACTCTACCCACGGCAAG-3′, 5′-CTGGAAGATGGTGATGGGTT-3′.

Immunoblotting analysis. Whole-cell extracts were prepared as described previously.[41] The protein concentration of the samples was determined using the Bradford method.[42] Samples were applied to polyacrylamide SDS gels, subjected to electrophoresis, and the resultant proteins immunoblotted with their respective antibodies.

Gelatin zymography. The proteolytic activity of MMP-9 and MMP-2 was assessed by SDS-PAGE using zymogram gels containing 0.1% gelatin, as described previously.[41] The FBS-free culture medium was concentrated and protein concentration determined according to the Bradford method.[42] After electrophoresis at 4°C, the gels were washed with 2.5% Triton X-100 for 30 min at room temperature and incubated with zymogram development buffer for 2 days at 37°C. Bands were visualized by staining with Coomassie Brilliant Blue.

Cell migration assay. *In vitro* wound-healing assays were used to assess cell migration as described previously,[43] using confluent A549 cells on a 24-well plate. Two linear wounds were scratched with a p200 pipette tip. The cell-free area was measured before and after 24 h of incubation (healing step) using NIH ImageJ software (NIH, Bethesda, ML, USA).

SiRNA targeting of genes. The siRNAs for DHODH and SIP1 were purchased from Qiagen. A549 cells were transfected with siRNA using HiPerFect transfection reagents according to the manufacturer's instructions. The siRNA *5′-UUCUCCGAACGUGUCACGUDTDT-3′* and *5′-ACGUGACACGUUCGGAGAADTDT-3′* was used as a nonspecific siRNA.

Administration of bleomycin, leflunomide and uridine. C57BL/6 mice maintained under chloral hydrate anesthesia (500 mg/kg) were administered one intratracheal injection of bleomycin (0.5 or 5 mg/kg) to induce fibrosis. Leflunomide (40 mg/kg) was dissolved in 1% methylcellulose and administered orally. Uridine (50 mg/kg) was dissolved in PBS and administered intratracheally.

Histological and immunohistochemical analyses. Lung tissue samples were fixed in 4% buffered paraformaldehyde and then embedded in paraffin before being cut into 4-μm-thick sections.

For histological examination, sections were stained first with Mayer's hematoxylin and then with 1% eosin alcohol solution. Samples were mounted with malinol and inspected using an Olympus BX51 microscope.

For Masson's trichrome staining of collagen, sections were sequentially treated with solution A (5% (w/v) potassium dichromate and 5% (w/v) trichloroacetic acid), Weigert's iron hematoxylin, solution B (1.25% (w/v) phosphotungstic acid and 1.25% (w/v) phosphomolybdic acid), 0.75% (w/v) Orange G solution, solution C (0.12% (w/v) xylidine ponceau, 0.04% (w/v) acid fuchsin and 0.02% (w/v) azophloxin), 2.5% (w/v) phosphotungstic acid, and finally Aniline Blue solution. Samples were mounted with malinol and inspected using an Olympus BX51 microscope.

For immunohistochemical analysis, sections were blocked with 3% goat serum for 15 min, incubated for 12 h with antibody against proSP-C and α-SMA in the presence of 2.5% BSA, and finally incubated for 3 h with Alexa Fluor 488 goat anti-rabbit IgG and Alexa Fluor 594 goat anti-mouse IgG in the presence of DAPI (5 μg/ml). Samples were mounted with VECTASHIELD and inspected using fluorescence microscopy (Olympus BX51) with deconvolution (Lumina Vision imaging software (Mitani Co., Tokyo, Japan)).

Hydroxyproline determination. Hydroxyproline content was determined as described previously.[44] Briefly, the right lung was removed and homogenized in 0.5 ml of 5% TCA. After centrifugation, pellets were hydrolyzed in 0.5 ml of 10 N HCl for 16 h at 110°C. Each sample was incubated for 20 min at room temperature after addition of 0.5 ml of 1.4% (w/v) chloramine T solution and then incubated at 65°C for 10 min after addition of 0.5 ml of Ehrlich's reagent (1 M DMBA, 70% (v/v) isopropanol and 30% (v/v) perchloric acid). Absorbance was measured at 550 nm, and the amount of hydroxyproline was determined.

Statistical analysis. Two-way analysis of variance (ANOVA), followed by Tukey's test or Student's *t*-test for unpaired results was used to evaluate differences between more than three groups or between two groups, respectively. Survival estimates were computed using standard Kaplan–Meier estimates with the log-rank test for the *P*-value of survival curves between BLM-treated mice with and without leflunomide administration. Differences were considered to be significant for values of $P<0.05$.

Conflict of interest

The authors declare no conflict of interest.

1. Olson AL, Swigris JJ, Lezotte DC, Norris JM, Wilson CG, Brown KK. Mortality from pulmonary fibrosis increased in the United States from 1992 to 2003. *Am J Respir Crit Care Med* 2007; **176**: 277–284.
2. Fumeaux T, Rothmeier C, Jolliet P. Outcome of mechanical ventilation for acute respiratory failure in patients with pulmonary fibrosis. *Intensive Care Med* 2001; **27**: 1868–1874.
3. Camus P, Fanton A, Bonniaud P, Camus C, Foucher P. Interstitial lung disease induced by drugs and radiation. *Respiration* 2004; **71**: 301–326.
4. Inoue A, Saijo Y, Maemondo M, Gomi K, Tokue Y, Kimura Y *et al.* Severe acute interstitial pneumonia and gefitinib. *Lancet* 2003; **361**: 137–139.
5. Flieder DB, Travis WD. Pathologic characteristics of drug-induced lung disease. *Clin Chest Med* 2004; **25**: 37–45.
6. Moore BB, Hogaboam CM. Murine models of pulmonary fibrosis. *Am J Physiol Lung Cell Mol Physiol* 2008; **294**: L152–L160.
7. Sheppard D. Transforming growth factor beta: a central modulator of pulmonary and airway inflammation and fibrosis. *Proc Am Thorac Soc* 2006; **3**: 413–417.
8. Kinnula VL, Myllarniemi M. Oxidant-antioxidant imbalance as a potential contributor to the progression of human pulmonary fibrosis. *Antioxid Redox Signal* 2008; **10**: 727–738.
9. Hinz B, Phan SH, Thannickal VJ, Galli A, Bochaton-Piallat ML, Gabbiani G. The myofibroblast: one function, multiple origins. *Am J Pathol* 2007; **170**: 1807–1816.
10. Gasse P, Mary C, Guenon I, Noulin N, Charron S, Schnyder-Candrian S *et al.* IL-1R1/MyD88 signaling and the inflammasome are essential in pulmonary inflammation and fibrosis in mice. *J Clin Invest* 2007; **117**: 3786–3799.
11. Kisseleva T, Brenner DA. Fibrogenesis of parenchymal organs. *Proc Am Thorac Soc* 2008; **5**: 338–342.
12. Willis BC, Borok Z. TGF-beta-induced EMT: mechanisms and implications for fibrotic lung disease. *Am J Physiol Lung Cell Mol Physiol* 2007; **293**: L525–L534.
13. Kasai H, Allen JT, Mason RM, Kamimura T, Zhang Z. TGF-beta1 induces human alveolar epithelial to mesenchymal cell transition (EMT). *Respir Res* 2005; **6**: 56.
14. Kim KK, Kugler MC, Wolters PJ, Robillard L, Galvez MG, Brumwell AN *et al.* Alveolar epithelial cell mesenchymal transition develops *in vivo* during pulmonary fibrosis and is regulated by the extracellular matrix. *Proc Natl Acad Sci USA* 2006; **103**: 13180–13185.
15. Kim KK, Wei Y, Szekeres C, Kugler MC, Wolters PJ, Hill ML *et al.* Epithelial cell alpha3beta1 integrin links beta-catenin and Smad signaling to promote myofibroblast formation and pulmonary fibrosis. *J Clin Invest* 2009; **119**: 213–224.
16. Smolen JS, Kalden JR, Scott DL, Rozman B, Kvien TK, Larsen A *et al.* Efficacy and safety of leflunomide compared with placebo and sulphasalazine in active rheumatoid arthritis: a double-blind, randomised, multicentre trial. European Leflunomide Study Group. *Lancet* 1999; **353**: 259–266.
17. Emery P, Breedveld FC, Lemmel EM, Kaltwasser JP, Dawes PT, Gomor B *et al.* A comparison of the efficacy and safety of leflunomide and methotrexate for the treatment of rheumatoid arthritis. *Rheumatology (Oxford)* 2000; **39**: 655–665.
18. Fox RI, Herrmann ML, Frangou CG, Wahl GM, Morris RE, Strand V *et al.* Mechanism of action for leflunomide in rheumatoid arthritis. *Clin Immunol* 1999; **93**: 198–208.
19. Scott DL. Interstitial lung disease and disease modifying anti-rheumatic drugs. *Lancet* 2004; **363**: 1239–1240.
20. Sakai F, Noma S, Kurihara Y, Yamada H, Azuma A, Kudoh S *et al.* Leflunomide-related lung injury in patients with rheumatoid arthritis: imaging features. *Mod Rheumatol* 2005; **15**: 173–179.
21. Mejlvang J, Kriajevska M, Vandewalle C, Chernova T, Sayan AE, Berx G *et al.* Direct repression of cyclin D1 by SIP1 attenuates cell cycle progression in cells undergoing an epithelial mesenchymal transition. *Mol Biol Cell* 2007; **18**: 4615–4624.
22. Thiery JP, Sleeman JP. Complex networks orchestrate epithelial-mesenchymal transitions. *Nat Rev Mol Cell Biol* 2006; **7**: 131–142.
23. Shirakihara T, Saitoh M, Miyazono K. Differential regulation of epithelial and mesenchymal markers by deltaEF1 proteins in epithelial mesenchymal transition induced by TGF-beta. *Mol Biol Cell* 2007; **18**: 3533–3544.
24. Saito RA, Watabe T, Horiguchi K, Kohyama T, Saitoh M, Nagase T *et al.* Thyroid transcription factor-1 inhibits transforming growth factor-beta-mediated epithelial-to-mesenchymal transition in lung adenocarcinoma cells. *Cancer Res* 2009; **69**: 2783–2791.
25. Li JL, Harris AL. Notch signaling from tumor cells: a new mechanism of angiogenesis. *Cancer Cell* 2005; **8**: 1–3.
26. Bray SJ. Notch signalling: a simple pathway becomes complex. *Nat Rev Mol Cell Biol* 2006; **7**: 678–689.
27. Sahlgren C, Gustafsson MV, Jin S, Poellinger L, Lendahl U. Notch signaling mediates hypoxia-induced tumor cell migration and invasion. *Proc Natl Acad Sci USA* 2008; **105**: 6392–6397.
28. Wang Z, Li Y, Kong D, Banerjee S, Ahmad A, Azmi AS *et al.* Acquisition of epithelial-mesenchymal transition phenotype of gemcitabine-resistant pancreatic cancer cells is linked with activation of the notch signaling pathway. *Cancer Res* 2009; **69**: 2400–2407.
29. Kuo EA, Hambleton PT, Kay DP, Evans PL, Matharu SS, Little E *et al.* Synthesis, structure-activity relationships, and pharmacokinetic properties of dihydroorotate dehydrogenase inhibitors: 2-cyano-3-cyclopropyl-3-hydroxy-N-[3′-methyl-4′-(trifluoromethyl)phenyl] propenamide and related compounds. *J Med Chem* 1996; **39**: 4608–4621.
30. Hatse S, De Clercq E, Balzarini J. Role of antimetabolites of purine and pyrimidine nucleotide metabolism in tumor cell differentiation. *Biochem Pharmacol* 1999; **58**: 539–555.
31. Yukawa E, Mori S, Ueda K, Nakada Y. Population pharmacokinetic investigation of low-dose methotrexate in rheumatoid arthritics Japanese patients. *J Clin Pharm Ther* 2007; **32**: 573–578.
32. Chan V, Charles BG, Tett SE. Population pharmacokinetics and association between A77 1726 plasma concentrations and disease activity measures following administration of leflunomide to people with rheumatoid arthritis. *Br J Clin Pharmacol* 2005; **60**: 257–264.
33. Baumann P, Mandl-Weber S, Volkl A, Adam C, Bumeder I, Oduncu F *et al.* Dihydroorotate dehydrogenase inhibitor A771726 (leflunomide) induces apoptosis and diminishes proliferation of multiple myeloma cells. *Mol Cancer Ther* 2009; **8**: 366–375.
34. Tang X, Yang J, Li J. Accelerative effect of leflunomide on recovery from hepatic fibrosis involves TRAIL-mediated hepatic stellate cell apoptosis. *Life Sci* 2009; **84**: 552–557.
35. Liu T, Hu B, Choi YY, Chung M, Ullenbruch M, Yu H *et al.* Notch1 signaling in FIZZ1 induction of myofibroblast differentiation. *Am J Pathol* 2009; **174**: 1745–1755.
36. Hamilton LC, Vojnovic I, Warner TD. A771726, the active metabolite of leflunomide, directly inhibits the activity of cyclo-oxygenase-2 *in vitro* and *in vivo* in a substrate-sensitive manner. *Br J Pharmacol* 1999; **127**: 1589–1596.
37. Xu X, Williams JW, Bremer EG, Finnegan A, Chong AS. Inhibition of protein tyrosine phosphorylation in T cells by a novel immunosuppressive agent, leflunomide. *J Biol Chem* 1995; **270**: 12398–12403.
38. Inokuma S, Sato T, Sagawa A, Matsuda T, Takemura T, Ohtsuka T *et al.* Proposals for leflunomide use to avoid lung injury in patients with rheumatoid arthritis. *Mod Rheumatol* 2008; **18**: 442–446.
39. Isohama Y, Kanemaru M, Kai H, Takahama K, Miyata T. Interaction between beta-adrenergic signaling and protein kinase C increases cytoplasmic Ca2+ in alveolar type II cells. *Life Sci* 2001; **68**: 2361–2371.
40. Isohama Y, Matsuo T, Kai H, Takahama K, Miyata T. Changes in beta 1- and beta 2-adrenoceptor mRNA levels in alveolar type II cells during cultivation. *Biochem Mol Biol Int* 1995; **36**: 561–568.
41. Namba T, Homan T, Nishimura T, Mima S, Hoshino T, Mizushima T. Up-regulation of S100P expression by non-steroidal anti-inflammatory drugs and its role in anti-tumorigenic effects. *J Biol Chem* 2009; **284**: 4158–4167.
42. Bradford MM. A rapid and sensitive method for the quantitation of microgram quantities of protein utilizing the principle of protein-dye binding. *Anal Biochem* 1976; **72**: 248–254.
43. Mima S, Tsutsumi S, Ushijima H, Takeda M, Fukuda I, Yokomizo K *et al.* Induction of claudin-4 by nonsteroidal anti-inflammatory drugs and its contribution to their chemopreventive effect. *Cancer Res* 2005; **65**: 1868–1876.
44. Woessner Jr JF. The determination of hydroxyproline in tissue and protein samples containing small proportions of this imino acid. *Arch Biochem Biophys* 1961; **93**: 440–447.

Supplementary Information accompanies the paper on Cell Death and Differentiation website (http://www.nature.com/cdd)

Biochemical Pharmacology 80 (2010) 920–931

Contents lists available at ScienceDirect

Biochemical Pharmacology

journal homepage: www.elsevier.com/locate/biochempharm

Heat shock protein 70 protects against bleomycin-induced pulmonary fibrosis in mice

Ken-Ichiro Tanaka [a], Yuta Tanaka [a], Takushi Namba [a], Arata Azuma [b], Tohru Mizushima [a,*]

[a] Graduate School of Medical and Pharmaceutical Sciences, Kumamoto University, 5-1 Oe-honmachi, Kumamoto 862-0973, Japan
[b] Department of Internal Medicine, Division of Respiratory, Infection and Oncology, Nippon Medical School, Tokyo 113-8602, Japan

ARTICLE INFO

Article history:
Received 25 March 2010
Accepted 24 May 2010

Keywords:
Heat shock protein 70
Bleomycin
Idiopathic pulmonary fibrosis
Geranylgeranylacetone
Epithelial–mesenchymal transition
Transforming growth factor-β1

ABSTRACT

Idiopathic pulmonary fibrosis (IPF) involves infiltration of leucocytes, pulmonary injury, fibrosis and resulting pulmonary dysfunction. Myofibroblasts and transforming growth factor (TGF)-β1 have been suggested to play a major role in the pathology and the myofibroblasts are derived from both lung epithelial cells through epithelial–mesenchymal transition (EMT) and activation of lung fibroblasts. Heat shock protein 70 (HSP70) confers protection against various stressors and has the anti-inflammatory activity. In this study, we examined the effect of expression of HSP70 on bleomycin-induced pulmonary fibrosis in mice, a tentative animal model of IPF. Bleomycin-induced pulmonary injury and inflammatory response were ameliorated in transgenic mice overexpressing HSP70 compared to wild-type mice, even though bleomycin-induced pulmonary fibrosis and dysfunction were also suppressed in the transgenic mice. The production of TGF-β1 and expression of pro-inflammatory cytokines was lower in cells from the transgenic mice than wild-type mice after the administration of bleomycin. *In vitro*, the suppression of HSP70 expression stimulated TGF-β1-induced EMT-like phenotypes of epithelial cells but did not affect the TGF-β1-dependent activation of fibroblasts. Orally administered geranylgeranylacetone (GGA), a clinically used drug with HSP-inducing activity, conferred protection against bleomycin-induced pulmonary injury, as well as against the inflammatory response, fibrosis and dysfunction. These results suggest that HSP70 plays a protective role against bleomycin-induced pulmonary injury, inflammation, fibrosis and dysfunction through cytoprotective effects and by inhibiting the production of TGF-β1, TGF-β1-dependent EMT of epithelial cells and expression of pro-inflammatory cytokines. Results also suggest that HSP70-inducing drugs, such as GGA, could be beneficial in the prophylaxis of IPF.

1. Introduction

Idiopathic pulmonary fibrosis (IPF) is a progressive and devastating chronic lung condition with poor prognosis; the reported mean length of survival from the time of diagnosis ranges from 2.8 to 4.2 years. IPF progresses insidiously and slowly, and acute exacerbation of IPF is a highly lethal clinical event [1,2]. As current agents for the treatment of IPF, such as steroids and immunosuppressors, have not been found to improve the prognosis [1,3,4], the development of new types of drugs to treat IPF is therefore required. To evaluate candidate drugs, the bleomycin-induced pulmonary fibrosis animal model provides a convenient option for the study of the disease given that it shares some characteristic features with IPF [5].

Although the etiology of IPF is not yet fully understood, recent studies have suggested that lung injury, inflammation (infiltration of leukocytes and activation of pro-inflammatory cytokines) and transforming growth factor (TGF)-β1 play an important role in IPF. Reactive oxygen species (ROS) that are released from the activated leukocytes cause further lung injury and inflammation. An increase in the number of lung myofibroblasts, an intermediate cell type between fibroblasts and smooth muscle cells, has been suggested to play an important role in the abnormal fibrosis and collagen deposition due to abnormal wound repair and remodelling; to this extent myofibroblasts produce considerable amounts of extracellular matrix components, such as collagen [6,7]. This abnormal process of fibrosis is responsible for the pulmonary dysfunction associated with IPF. It was previously believed that the origin of myofibroblasts was solely peribronchiolar and that perivascular fibroblasts transdifferentiate to myofibroblasts in response to various stimuli, in particular TGF-β1 [8]. However, recently it was revealed that lung epithelial cells undergo epithelial–mesenchymal transition (EMT) to become myofibroblasts after treatment with TGF-β1 *in vitro* [9–11]. EMT of lung epithelial cells also seems to be induced in the lungs of IPF patients and bleomycin-treated animals [9,12–14]. Furthermore, inhibition of EMT by knockout of

* Corresponding author. Tel.: +81 96 371 4323; fax: +81 96 371 4323.
E-mail address: mizu@gpo.kumamoto-u.ac.jp (T. Mizushima).

0006-2952/$ – see front matter © 2010 Elsevier Inc. All rights reserved.
doi:10.1016/j.bcp.2010.05.025

the *integrin-α3* gene has been shown to suppress bleomycin-induced pulmonary fibrosis in mice [15]. Therefore, drugs that inhibit the production of TGF-β1 and/or the EMT of lung epithelial cells could potentially be therapeutically beneficial against IPF.

Different stressors induce cells to express heat shock proteins (HSPs). The expression of HSPs, especially HSP70, in cultured cells protects these cells against a range of stressors, including ROS [16]. Interestingly, geranylgeranylacetone (GGA), a leading anti-ulcer drug on the Japanese market, has been reported to be a non-toxic HSP-inducer [17]. In addition to the cytoprotective effects of HSP70, its anti-inflammatory effects have been identified recently [18]. Thus, it is reasonable to speculate that HSP70 could protect against lung diseases such as acute respiratory distress syndrome (ARDS) and IPF. In fact, induction of the expression of HSP70 at the lung by whole-body heat treatment or by adenovirus with the *hsp70* gene protected against lipopolysaccharide (LPS)-induced or cecal ligation and puncture (CLP)-induced lung damage, respectively, both of which are animal models of ARDS [19–21]. Furthermore, HSP70-deficient mice were reported to be sensitive to CLP-induced lung damage [22]. However, the effect of HSP70 expression on IPF-related fibrosis has not been tested. In this study, we show that bleomycin-induced lung injury, inflammation, fibrosis and dysfunction were suppressed in transgenic mice overexpressing HSP70. Furthermore, orally administered GGA conferred protection against these bleomycin-induced pulmonary alterations, suggesting that HSP70-inducing drugs could be beneficial against prophylaxis of IPF.

2. Materials and methods

2.1. Chemicals and animals

Paraformaldehyde, fetal bovine serum (FBS), 4-(Dimethylamino)-benzaldehyde (DMBA), chloramine T, potassium dichromate, phosphotungstic acid, phosphomolybdic acid, Orange G and acid fuchsin were obtained from Sigma (St. Louis, MO). Antibodies against HSP25, HSP47, HSP60, HSP70 (for immunohistochemical analysis), HSP90 or α-smooth muscle actin (α-SMA) were purchased from Stressgen (Ann Arbor, MI) or Abcam (Cambridge, Cambridgeshire). Antibodies against actin and E-cadherin were purchased from Santa Cruz Biotechnology (Santa Cruz, CA). An ELISA kit for TGF-β1 and an antibody against HSP70 (for immunoblotting) were from R&D systems, Inc. (Minneapolis, MN). Bleomycin was from Nippon Kayaku (Tokyo, Japan). Novoheparin (5000 units) for injection was from Mochida Pharmaceutical Co. (Tokyo, Japan). Chloral hydrate was from Nacalai Tesque (Kyoto, Japan). Diff-Quik was from the Sysmex Corporation (Kobe, Japan). Terminal deoxynucleotidyl transferase (TdTase) was obtained from TOYOBO (Osaka, Japan). Biotin 14-ATP, Alexa Fluor 594 goat anti-rabbit immunoglobulin G and Alexa Fluor 488 conjugated with streptavidin were purchased from Invitrogen (Carlsbad, CA). Mounting medium for immunohistochemical analysis (VECTASHIELD) was from Vector Laboratories (Burlingame, CA). Cytospin® 4 was purchased from Thermo Electron Corporation (MA, USA), while quercetin, TGF-β1, L-hydroxyproline, sodium acetate, trichloroacetic acid (TCA), azophloxin and aniline blue were from WAKO Pure Chemicals (Tokyo, Japan). Xylidine ponceau was from WALDECK GmbH & Co. KG, DIVISION CHROMA (Muenster, Germany), and Mayer's hematoxylin, 1% eosin alcohol solution, mounting medium for histological examination (malinol) and Weigert's iron hematoxylin were from MUTO Pure Chemicals (Tokyo, Japan). 4,6-Diamino-2-phenylindole (DAPI) was from Dojindo (Kumamoto, Japan). Transgenic mice overexpressing HSP70 and their wild-type counterparts (6–8 weeks old, male) were gifts from Drs. C.E. Angelidis and G.N. Pagoulatos (University of Ioannina, Ioannina, Greece) and were prepared as described previously [23]. Homozygotic transgenic mice overexpressing HSP70 were used in experiments. The experiments and procedures described here were carried out in accordance with the Guide for the Care and Use of Laboratory Animals as adopted and promulgated by the National Institutes of Health, and were approved by the Animal Care Committee of Kumamoto University.

2.2. Administration of bleomycin and preparation of bronchoalveolar lavage fluid (BALF) and cell count

Mice were maintained under anaesthesia with chloral hydrate (500 mg/kg) and were given one intratracheal injection of bleomycin (5 mg/kg) to induce an inflammatory response and fibrosis.

BALF was collected by cannulating the trachea and lavaging the lung with 1 ml of sterile PBS containing 50 units/ml heparin (two times). About 1.8 ml of BALF was routinely recovered from each animal. The total cell number was counted using a hemocytometer. Cells were stained with Diff-Quik reagents and the ratios of alveolar macrophages, lymphocytes and neutrophils to total cells were determined. More than 200 cells were counted for each sample.

2.3. Histological and immunohistochemical analyses and terminal deoxynucleotidyl transferase dUTP nick-end labeling (TUNEL) assay

Lung tissue samples were fixed in 4% buffered paraformaldehyde and then embedded in paraffin before being cut into 4 μm-thick sections.

For histological examination, sections were stained first with Mayer's hematoxylin and then with 1% eosin alcohol solution. Samples were mounted with malinol and inspected with the aid of an Olympus BX51 microscope (Tokyo, Japan).

For staining of collagen (Masson's trichrome staining), sections were treated sequentially with solution A (5% (w/v) potassium dichromate and 5% (w/v) trichloroacetic acid), Weigert's iron hematoxylin, solution B (1.25% (w/v) phosphotungstic acid and 1.25% (w/v) phosphomolybdic acid), 0.75% (w/v) Orange G solution, solution C (0.12% (w/v) xylidine ponceau, 0.04% (w/v) acid fuchsin and 0.02% (w/v) azophloxin), 2.5% (w/v) phosphotungstic acid, and finally Aniline Blue solution. Samples were mounted with malinol and inspected with the aid of an Olympus BX51 microscope.

For immunohistochemical analysis, sections were treated with 20 μg/ml Protease K for antigen activation and incubated with 0.3% hydrogen peroxide in methanol for removal of endogenous peroxidase. Sections were blocked with 2.5% goat serum for 10 min, incubated for 12 h with an antibody against HSP70 (1:200 dilution) in the presence of 2.5% bovine serum albumin (BSA) and then incubated for 1 h with peroxidase-labeled polymer conjugated to goat anti-mouse immunoglobulins. Then, 3,3′-diaminobenzidine was applied to the sections and the sections were finally incubated with Mayer's hematoxylin. Samples were mounted with malinol and inspected using a fluorescence microscope (Olympus BX51).

For the TUNEL assay, sections were incubated first with proteinase K (20 μg/ml) for 15 min at 37 °C, then with TdTase and biotin 14-ATP for 1 h at 37 °C and finally with Alexa Fluor 488 conjugated with streptavidin and DAPI (5 μg/ml) for 2 h. Samples were mounted with VECTASHIELD and inspected with the aid of a fluorescence microscope (Olympus BX51).

2.4. Hydroxyproline determination

Hydroxyproline content was determined as described [24]. Briefly, the right lung was removed and homogenized in 0.5 ml of 5% TCA. After centrifugation, pellets were hydrolysed in 0.5 ml of

10 N HCl for 16 h at 110 °C. Each sample was incubated for 20 min at room temperature after the addition of 0.5 ml of 1.4% (w/v) chloramine T solution and then incubated at 65 °C for 10 min after the addition of 0.5 ml of Ehrlich's reagent (1 M DMBA, 70% (v/v) isopropanol and 30% (v/v) perchloric acid). Absorbance was measured at 550 nm, and the amount of hydroxyproline was determined.

2.5. Real-time RT-PCR analysis

Real-time RT-PCR was performed as previously described [25] with some modifications. Total RNA was extracted from cells using an RNeasy kit according to the manufacturer's protocol. Samples (2.5 μg RNA) were reverse-transcribed using a first-strand cDNA synthesis kit. Synthesized cDNA was used in real-time RT-PCR (Chromo 4 instrument (Bio-Rad Laboratories, Hercules, CA)) experiments using iQ SYBR GREEN Supermix, and analyzed with Opticon Monitor Software. Specificity was confirmed by electrophoretic analysis of the reaction products and by inclusion of template- or reverse transcriptase-free controls. To normalize the amount of total RNA present in each reaction, actin cDNA was used as an internal standard.

Primers were designed using the Primer3 website (http://frodo.wi.mit.edu/cgi-bin/primer3/primer3_www.cgi). The primers used were (name: forward primer, reverse primer): for human, *col1a1*: 5′-ccctgtctgcttcctgtaaact-3′, 5′-catgttcggttggtcaaagata-3′; *E-cadherin*: 5′-tgcccagaaaatgaaaaagg-3′, 5′-gtgtatgtggcaatgcgttc-3′; *hsp47*: 5′-ccatgttcttcaagccacact-3′, 5′-cgtagtagttgtagaggcctgt-3′; *hsp70*: 5′-aggccaacaagatcaccatc-3′, 5′-tcgtcctccgctttgtactt-3′; *slug*: 5′-gagcatttgcagacaggtca-3′, 5′-acagcagccagattcctcat-3′; *α-sma*: 5′-catcatgcgtctggatctgg-3′, 5′-ggacaatctcacgctcagca-3′; *actin*: 5′-ggacttcgagcaagagatgg-3′, 5′- agcactgtgttggcgtacag-3′. For mouse, *tumor necrosis factor (tnf)-α*: 5′-cgtcagccgatttgctatct-3′, 5′-cggactccgcaaagtctaag-3′; *interleukin (il)-1β*: 5′-gatcccaagcaatacccaaa-3′, 5′-ggggaactctgcagactcaa-3′; *il-6*: 5′-ctggagtcacagaaggagtgg-3′, 5′-ggtttgccgagtagatctcaa-3′; *gapdh*: 5′-aactttggcattgtggaagg-3′, 5′-acacattgggggtaggaaca-3′.

The amount of TGF-β1 in the lung tissue was also measured by ELISA according to the manufacturer's protocol.

2.6. Analysis of lung function

Analysis of lung function was performed with a computer-controlled small-animal ventilator (FlexiVent; SCIREQ, Montreal, Canada), as described previously [26]. Mice were anesthetized with chloral hydrate (500 mg/kg), tracheotomised with an 8 mm section of metallic tubing, and mechanically ventilated at a rate of 150 breaths/min, using a tidal volume of 8.7 ml/kg and a positive end-expiratory pressure of 2–3 cm H_2O. The single-compartment model (snap shot) and the constant-phase model (forced oscillation technique (FOT)) were applied to analyse lung function. Total respiratory system compliance or total respiratory system elastance and tissue elastance were measured by snap shot or FOT, respectively. All data were analysed using FlexiVent software (version 5.3).

2.7. Cell culture and immunostaining

A549 cells were cultured in DMEM medium supplemented with 10% FBS in a humidified atmosphere of 95% air with 5% CO_2 at 37 °C.

For immunostaining, A549 cells were grown in the Lab-Tek II chamber slide system (Nalge Nunc International, Rochester, NY). Cells were fixed in 4% buffered paraformaldehyde for 20 min, blocked with goat serum for 15 min, then incubated for 1 h with antibody against E-cadherin or α-SMA in the presence of 2.5% bovine serum albumin, before finally being incubated for 2 h with Alexa Fluor 488 goat anti-mouse IgG. Samples were mounted with VECTASHIELD. Images were captured on a fluorescence microscope (Olympus BX51).

2.8. Statistical analysis

All values are expressed as the mean ± S.E.M. The Tukey test or the Student's *t*-test for unpaired results was used to evaluate differences between more than three groups or between two groups, respectively. Differences were considered to be significant for values of $P < 0.05$.

3. Results

3.1. Effect of HSP70 on bleomycin-induced pulmonary damage and fibrosis

Pulmonary fibrosis was induced in wild-type mice and transgenic mice overexpressing HSP70 (mice that overexpress human HSP70 under the control of the human β-actin promoter [27]) that had been given a once-only (at day 0) intratracheal administration of bleomycin. First, we monitored the expression of HSPs in lung tissues by immunoblotting. As shown in Fig. 1A and B, the transgenic mice showed higher levels of expression of HSP70 in the lung than did wild-type mice in the presence and absence of bleomycin treatment. There was no clear difference in the expression of HSPs other than HSP70 between transgenic mice and wild-type mice (Fig. 1A and B). We used an antibody against human HSP70 for immunoblotting. Since HSP70 has a high homology (more than 90%) between mouse and human, it may cross-react to mouse HSP70. Results in Fig. 1A support this notion. However, the relative efficiency of recognition for mouse HSP to that for human HP70 has not examined, thus we could not compare the extent of expression of HSP70 between wild-type mice and the transgenic mice. The administration of bleomycin increased the expression of HSP47 as described previously [28], but did not affect the expression of other HSPs, including HSP70 (Fig. 1A and B).

The bleomycin-induced inflammatory response can be monitored as a function of the number of inflammatory cells (alveolar macrophages, lymphocytes and neutrophils) in BALF 3 days after the administration of bleomycin. As shown in Fig. 2A, the total number of inflammatory cells and individual numbers of alveolar macrophages, lymphocytes and neutrophils were all increased by the bleomycin treatment. Compared to wild-type mice, this increase was suppressed in transgenic mice overexpressing HSP70, although differences in the numbers of alveolar macrophages and lymphocytes were not statistically significant between wild-type and transgenic mice in response to bleomycin treatment (Fig. 2A). Histopathological analysis of pulmonary tissues with the aid of hematoxylin and eosin (H & E) staining revealed that the bleomycin-induced pulmonary damage was ameliorated in transgenic mice overexpressing HSP70 compared to wild-type mice (Fig. 2B). Furthermore, the bleomycin-induced increase in the number of TUNEL-positive cells in pulmonary tissues (indicative of apoptosis) was also suppressed in transgenic mice overexpressing HSP70 (Fig. 2C and D). These results suggest that expression of HSP70 suppresses the bleomycin-induced pulmonary inflammatory response and tissue damage.

Bleomycin-induced pulmonary fibrosis can be monitored by histopathological analysis and measurement of hydroxyproline levels (an indicator of collagen levels), 14 days after the administration of bleomycin. Masson's trichrome staining of collagen showed that bleomycin administration induced collagen deposition in wild-type mice and that the extent of this deposition was suppressed in transgenic mice overexpressing HSP70 (Fig. 3A).

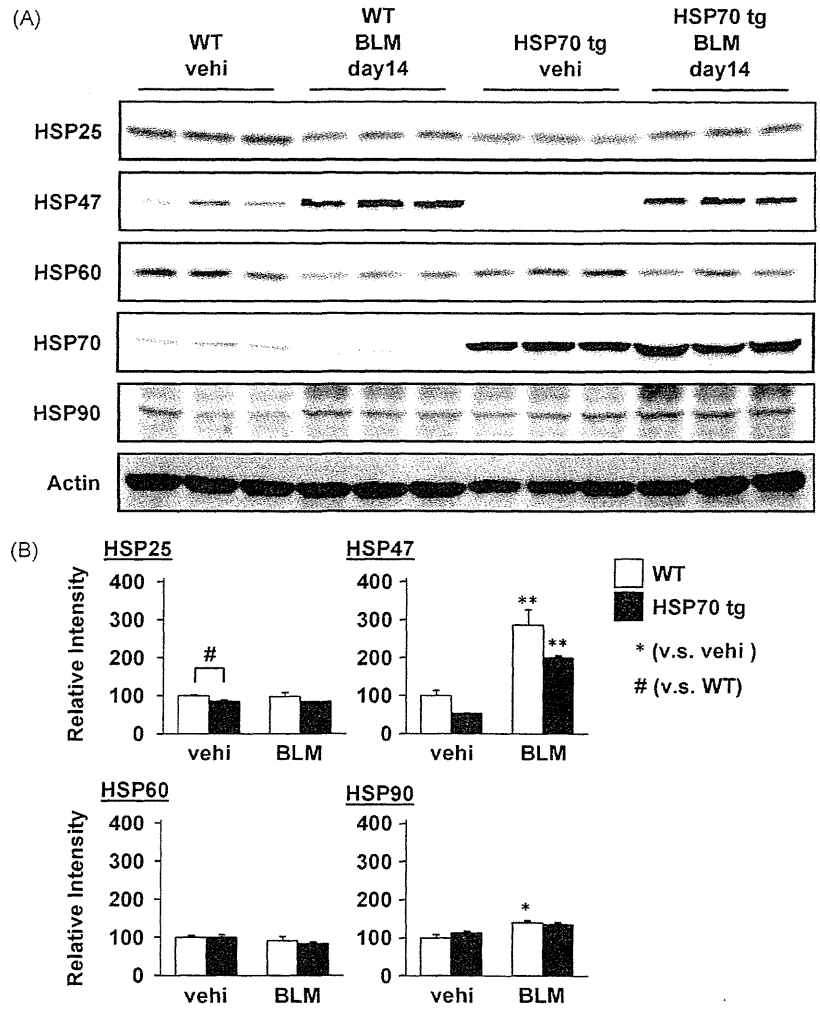

Fig. 1. Expression of HSPs in lung tissues after administration of bleomycin. Transgenic mice overexpressing HSP70 (HSP70 tg) and wild-type (WT) mice were treated with (BLM) or without (vehi) bleomycin (5 mg/kg) once-only at day 0. At day 14, lung tissues were removed and protein was extracted. Samples were analysed by immunoblotting with an antibody against HSP25, HSP47, HSP60, HSP70, HSP90 or actin (A). The band intensity of each HSP (except HSP70) was determined and normalized with its respective actin intensity (B). Values shown are mean ± S.E.M. ($n = 3$). * or $^{\#}P < 0.05$; ** or $^{\#\#}P < 0.01$.

H & E staining revealed that a low level of bleomycin-induced pulmonary damage in transgenic mice was evident 14 days after the administration of bleomycin (Fig. 3A). Bleomycin also increased pulmonary hydroxyproline levels, although to a lesser degree in transgenic mice compared to wild-type mice (Fig. 3B). These results suggest that bleomycin-induced pulmonary fibrosis is decreased by the expression of HSP70.

Myofibroblasts was monitored by immunohistochemical analysis with an antibody against α-SMA, a myofibroblast marker. As shown in Fig. 3C, a bleomycin-dependent increase in the expression of α-SMA was suppressed in transgenic mice overexpressing HSP70 compared to wild-type mice, suggesting that expression of HSP70 also suppresses the bleomycin-dependent increase in pulmonary myofibroblast number.

In humans, pulmonary fibrosis leads to an alteration in lung mechanics characterised by a decrease in compliance and an increase in elastance [26,29]. We thus examined the effect of HSP70 expression on bleomycin-induced alterations to lung mechanics, using a computer-controlled small-animal ventilator. Total respiratory system compliance was decreased as a consequence of bleomycin treatment in wild-type mice and this index was significantly higher in bleomycin-administered transgenic mice overexpressing HSP70 than bleomycin-administered wild-type mice (Fig. 3D). Total respiratory system elastance (elastance of total lung including bronchi, bronchiole and alveoli) and tissue elastance (elastance of alveoli) were increased in response to bleomycin treatment in wild-type mice, and these indexes were significantly lower in similarly treated transgenic mice overexpressing HSP70 (Fig. 3D). These results suggest that bleomycin-induced pulmonary dysfunction is improved under conditions of HSP70 expression.

3.2. Mechanism for the inhibitory effect of HSP70 on bleomycin-induced pulmonary fibrosis

As described above, TGF-β1 plays an important role in bleomycin-induced pulmonary fibrosis. Thus, as a first step to reveal the mechanism underlying the inhibitory effect of HSP70 on bleomycin-induced pulmonary fibrosis, the production of TGF-β1 in cells contained in BALF was compared between bleomycin-administered wild-type mice and transgenic mice overexpressing HSP70. As shown in Fig. 4A, the level of TGF-β1 production was lower in cells prepared from BALF of transgenic mice compared to wild-type mice, both with and without prior bleomycin treatment. As such, bleomycin enhanced the production of TGF-β1 in cells from BALF of wild-type mice but not in those from the transgenic mice (Fig. 4A).

We also compared the bleomycin-induced expression of pro-inflammatory cytokines in cells present in BALF. As shown in Fig. 4B, the mRNA expression of pro-inflammatory cytokines (TNF-α, IL-1β and IL-6) was clearly induced by the administration of

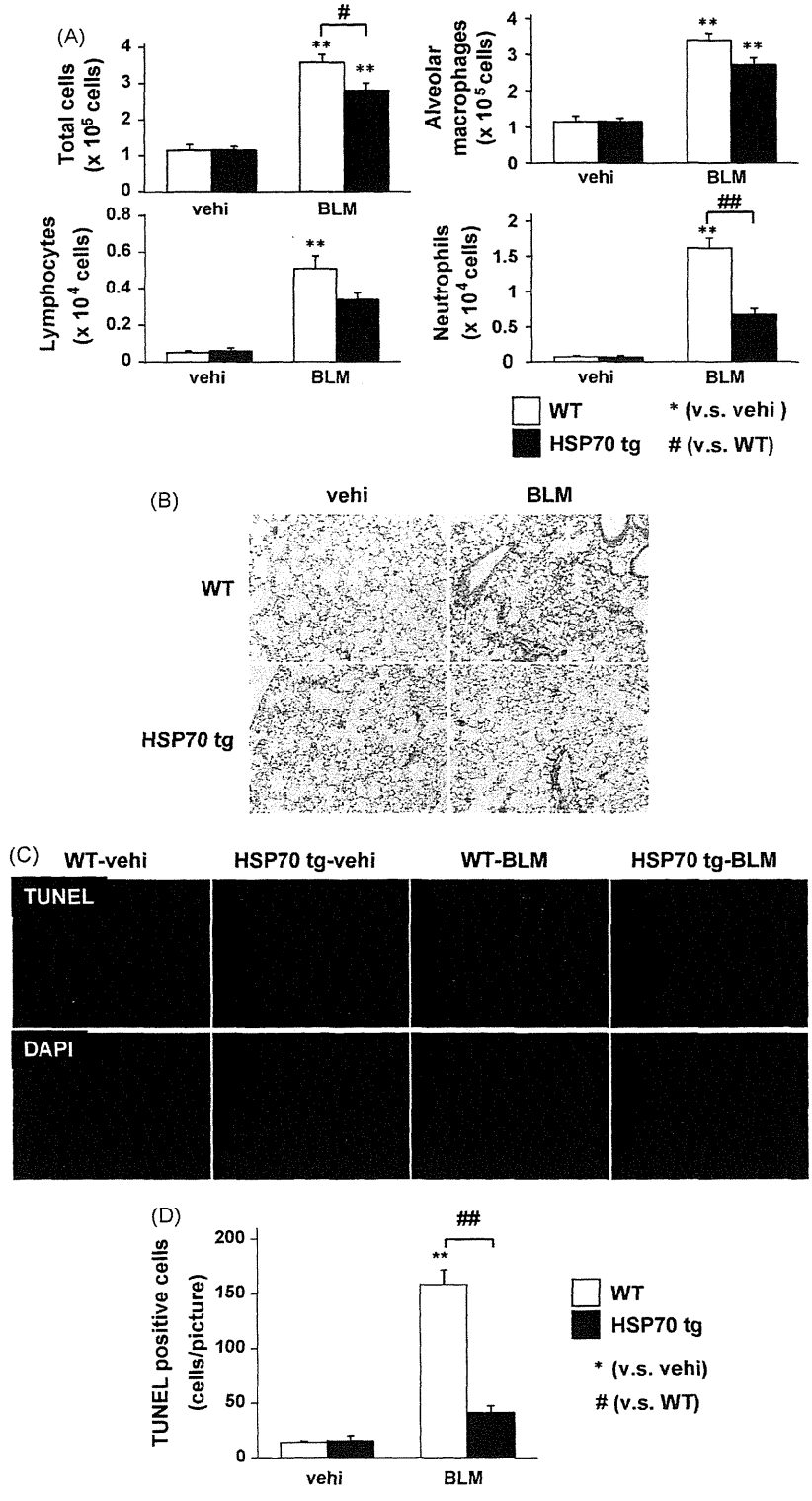

Fig. 2. Bleomycin-induced pulmonary inflammatory response and damage in transgenic mice overexpressing HSP70. Transgenic mice overexpressing HSP70 (HSP70 tg) and wild-type (WT) mice were treated with (BLM) or without (vehi) bleomycin (5 mg/kg) once-only at day 0. At day 3, total cell number, and individual numbers of alveolar macrophages, lymphocytes and neutrophils in BALF were determined as described in Section 2 (A). Sections of pulmonary tissue were prepared at day 3 and subjected to histopathological examination (H & E staining) (B) or TUNEL assay and DAPI staining (C). TUNEL-positive cells in the three sections were counted (D). Values shown are mean ± S.E.M. ($n = 3$–13). $^{\#}P < 0.05$; ** or $^{\#\#}P < 0.01$.

bleomycin and this expression was lower in cells in BALF prepared from the transgenic mice compared to wild-type mice. The results in Fig. 4 suggest that the decreased production of TGF-β1 and expression of pro-inflammatory cytokines in bleomycin-treated transgenic mice overexpressing HSP70 is responsible for their resistance to bleomycin-induced pulmonary fibrosis.

As described in Section 1, an increase in the number of pulmonary myofibroblasts associated with fibrosis is due to the stimulation of EMT of epithelial cells and the activation of fibroblasts. Thus, the results in Fig. 3C suggest that the TGF-β1-dependent EMT of lung epithelial cells and/or activation of fibroblasts are/is suppressed by the expression of HSP70. To test

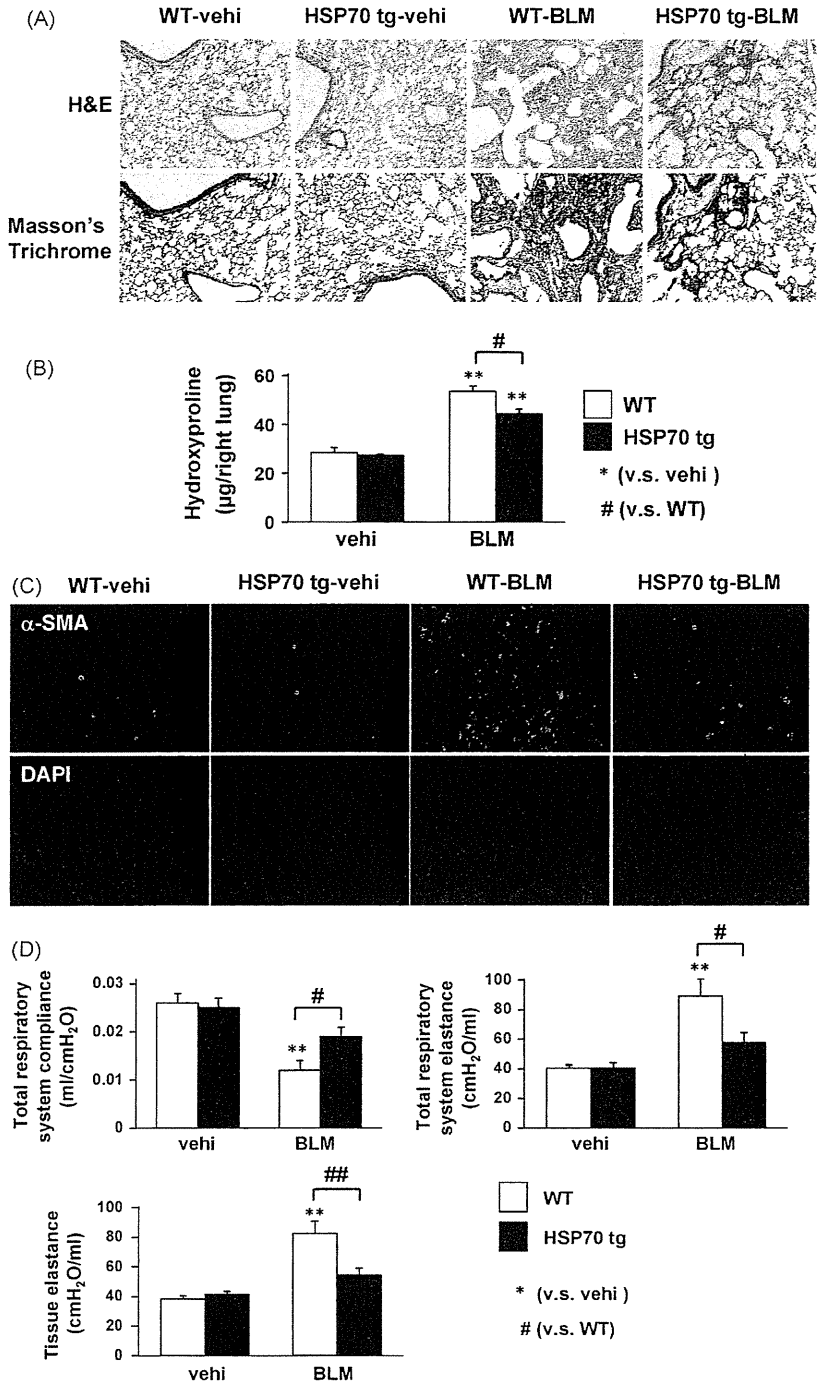

Fig. 3. Bleomycin-induced pulmonary fibrosis and dysfunction in transgenic mice overexpressing HSP70. Transgenic mice overexpressing HSP70 (HSP70 tg) and wild-type (WT) mice were treated with (BLM) or without (vehi) bleomycin (5 mg/kg) once-only at day 0. At day 14, sections of pulmonary tissue were prepared (A and C). The sections were subjected to histopathological examination (H & E staining and Masson's trichrome staining) (A). The pulmonary hydroxyproline level was determined at day 14 as described in Section 2 (B). The sections were subjected to immunohistochemical analysis with an antibody against α-SMA (C). At day 14, total respiratory system compliance, total respiratory system elastance and tissue elastance were determined as described in Section 2 (D). Values shown are mean ± S.E.M. ($n = 3$–7). $^{\#}P < 0.05$; ** or $^{\#\#}P < 0.01$.

this idea *in vitro*, we examined the effect of siRNA for HSP70 (we could not overexpress HSP70 by plasmids under the conditions) on the TGF-β1-dependent alteration of expression of EMT-related genes in cultured human type II alveolar (A549) cells. Treatment of cells with TGF-β1 down-regulated the expression of a marker of epithelial cells (*E-cadherin*) and up-regulated the expression of a marker of myofibroblasts (*col1a1* (one of the genes for collagen I)) (Fig. 5A), suggesting that TGF-β1-induced the EMT of A549 cells. The down-regulation of expression of E-cadherin by TGF-β1 was also observed at protein level (Fig. 5B). TGF-β1 did not alter the expression of *α-sma* mRNA under these experimental conditions (Fig. 5A). Transfection of cells with siRNA for HSP70 not only suppressed the expression of *hsp70* mRNA and HSP70 protein in the presence and absence of TGF-β1 but also suppressed the expression of *E-cadherin* mRNA and E-cadherin protein and induced the expression of *α-sma* and *col1a1* mRNAs in the presence of TGF-β1 (Fig. 5A and B). The siRNA also affected the background expression of *E-cadherin* and *α-sma* mRNAs and E-cadherin protein (Fig. 5A and B). Suppression or induction of expression of E-cadherin and α-SMA, respectively, by either treatment with TGF-β1 or transfection with siRNA for HSP70 was also confirmed by immunostaining analysis (Fig. 5C and D). As

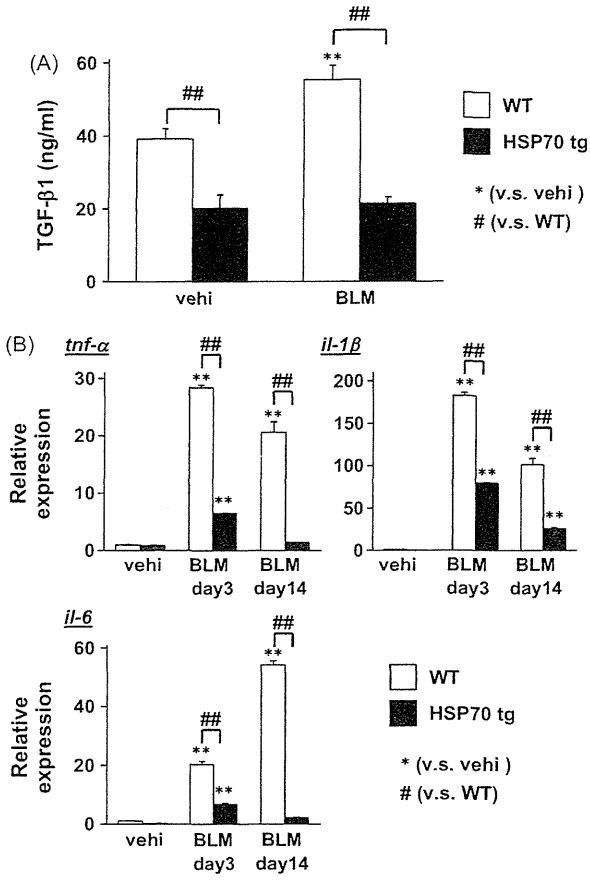

Fig. 4. Effect of expression of HSP70 on production of TGF-β1 and expression of pro-inflammatory cytokines. Transgenic mice overexpressing HSP70 (HSP70 tg) and wild-type (WT) mice were treated with (BLM) or without (vehi) bleomycin (5 mg/kg) once-only at day 0 and cells in BALF were collected at day 3 (A and B). Cells were incubated for 24 h and the level of TGF-β1 in the culture medium was determined by ELISA (A). Total RNA was extracted and subjected to real-time RT-PCR using a specific primer set for each gene. Values were normalized to the *gapdh* gene and expressed relative to the control sample (B). Values shown are mean ± S.E.M. ($n = 3$–6). ** or ## $P < 0.01$.

shown in Fig. 5E, either treatment with TGF-β1 or transfection with siRNA for HSP70 induced morphological change (from a cobble-stone-like epithelial monolayer to dispersed spindle-shaped mesenchymal cells with reduced cell-cell contact), one of characteristic features of induction of EMT.

A number of transcription factors (such as Slug) are involved in the induction of EMT [30,31]. We found that the transfection of cells with siRNA for HSP70 enhanced the expression of *slug* mRNA in the presence and absence of TGF-β1 (Fig. 5A). The results in Fig. 5 suggest that the expression of HSP70 suppresses the bleomycin-induced EMT of A549 cells by suppressing the expression of Slug.

We also examined the effect of HSP70 expression on the TGF-β1-dependent activation of lung fibroblasts *in vitro*. Treatment of HFL-1 cells (human embryonic lung fibroblasts) with TGF-β1-induced the expression of *col1a1*, *α-sma* and *hsp47* mRNAs and collagen I protein (Fig. 6A and B), suggesting that TGF-β1 activated fibroblasts to myofibroblasts. The transfection of cells with siRNA for HSP70 did not affect the TGF-β1-dependent alteration in expression of these genes (Fig. 6A and B), suggesting that the expression of HSP70 did not affect the TGF-β1-dependent activation of fibroblasts.

3.3. Effect of GGA on bleomycin-induced pulmonary fibrosis

We subsequently examined the effect of GGA on bleomycin-induced pulmonary damage, inflammatory response, fibrosis and dysfunction. Oral administration of GGA suppressed the bleomycin-induced increase in the number of inflammatory cells present in BALF (Fig. 7A), and decreased pulmonary damage (Fig. 7B) and epithelial apoptosis (Fig. 7C and D) 3 days after the administration of bleomycin. Immunohistochemical analysis with an antibody against HSP70 revealed that treatment with bleomycin slightly induced the pulmonary expression of HSP70, and the simultaneous administration of GGA enhanced this expression (Fig. 7E). The extent of bleomycin-induced pulmonary fibrosis 14 days after the administration of bleomycin was also reduced by the administration of GGA; GGA suppressed both the bleomycin-induced collagen deposition and the increase in pulmonary hydroxyproline content (Fig. 7F and G).

We also examined the effect of GGA on bleomycin-induced alterations to lung mechanics. As shown in Fig. 7H, the bleomycin-induced decrease in total respiratory system compliance and the increase in total respiratory system elastance and tissue elastance were significantly suppressed by the administration of GGA, suggesting that GGA exerts a protective effect against bleomycin-induced lung dysfunction. Taking these findings with the results shown in Figs. 2 and 3, it is likely that GGA suppresses the negative effects of bleomycin and improves lung function by inducing HSP70 expression.

In order to test this idea, we examined the effect of quercetin, an inhibitor for HSP70, on the ameliorative effect of GGA for bleomycin-induced pulmonary fibrosis and dysfunction. As shown in Fig. 7F–H, the ameliorative effect of GGA on bleomycin-induced pulmonary fibrosis and dysfunction was not observed in the presence of simultaneous administration of quercetin, suggesting that GGA suppresses bleomycin-induced pulmonary fibrosis and dysfunction by inducing HSP70 expression.

4. Discussion

An ameliorative effect of HSP70 due to its cytoprotective, anti-inflammatory and molecular chaperone (quality control of proteins) properties has been reported for animal models of various diseases. For example, using transgenic mice over-expressing HSP70, we have reported that HSP70 protects against irritant-produced lesions in the stomach and small intestine, inflammatory bowel disease-related experimental colitis and ultraviolet (UV)-induced skin damage [23,32–35]. The potential therapeutic applicability of HSP70 for use in other diseases, such as neurodegenerative diseases, ischemia-reperfusion damage and diabetes has also been suggested [36–38]. Interestingly, GGA, an anti-ulcer drug and HSP-inducer has been reported to suppress not only gastric lesions but also lesions of the small intestine, inflammatory bowel disease-related experimental colitis and neurodegenerative diseases [32,34,37,39]. On the other hand, the role of HSP70 in IPF has not been fully evaluated. It was recently reported that oral administration of GGA suppresses bleomycin-induced pulmonary fibrosis [40]. However, because GGA induces expression of HSPs other than HSP70, and has various pharmacological activities other than induction of HSPs (such as an increase in blood flow, stimulation of surface mucus production and direct protection of cell membranes [41–43]), it remains unclear whether GGA achieves its anti-fibrotic activity through up-regulation of expression of HSP70. In this study, we used transgenic mice overexpressing HSP70 to identify the role of HSP70 in bleomycin-induced pulmonary fibrosis and found that the transgenic mice showed a phenotypic resistance to this treatment. This is the first genetic evidence of the protective role of HSP70 against IPF-related fibrosis. The results presented here also suggest that GGA achieves its anti-fibrotic activity via the up-regulation of HSP70 expression.

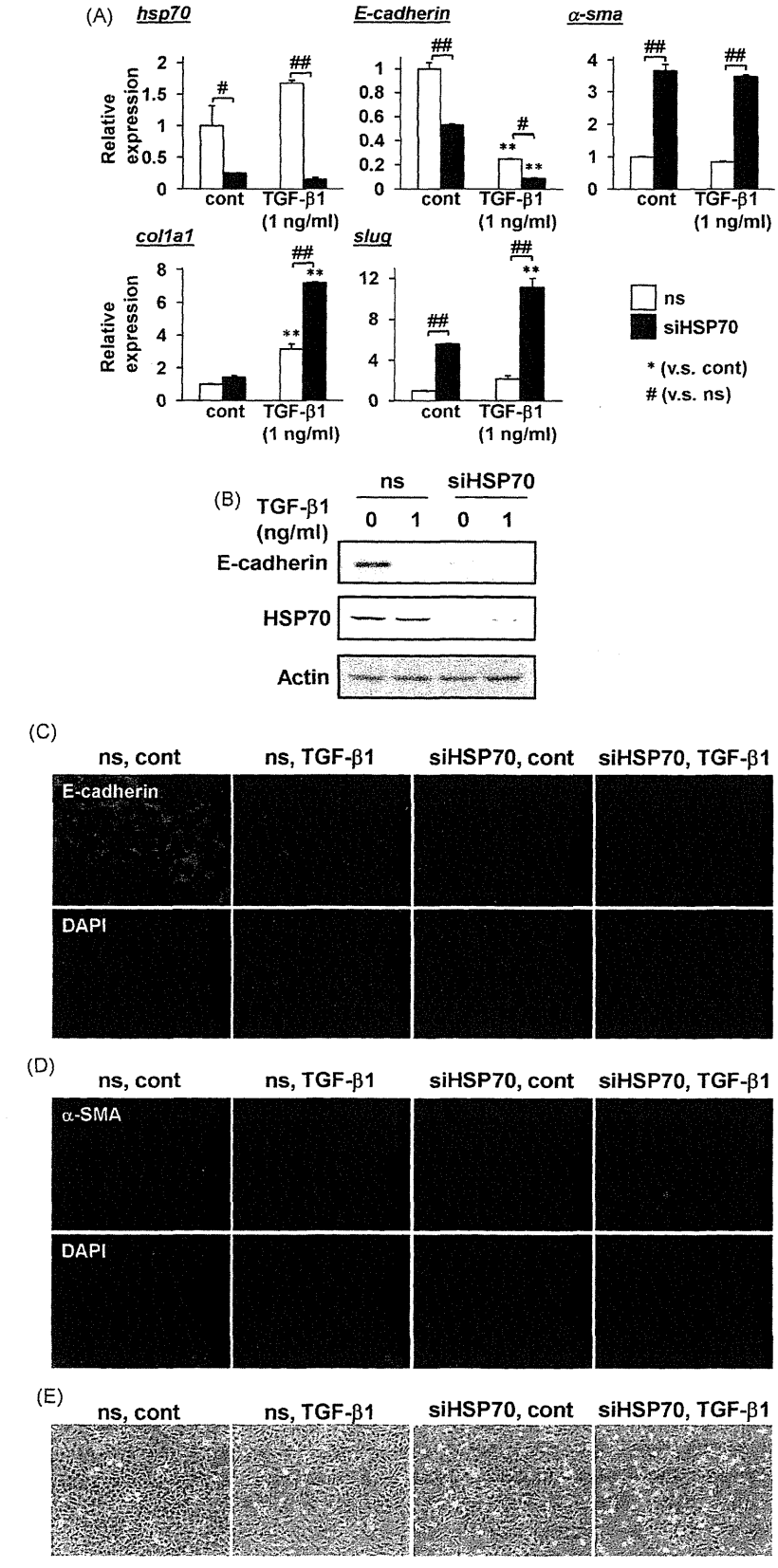

Fig. 5. Effect of siRNA for HSP70 on TGF-β1-induced EMT-like phenotypes. A549 cells were transfected with 1.2 μg of siRNA for HSP70 (siHSP70) or non-silencing (ns) siRNA and incubated for 24 h. Cells were then incubated with the indicated concentration of TGF-β1 for 48 h. Expression of each gene was examined by real-time RT-PCR as described in the legend of Fig. 4 (A). Expression of each protein was examined by immunoblotting as described in the legend of Fig. 1 (B). Immunostaining with an antibody against E-cadherin (C) or α-SMA (D) was done as described in Section 2. Cell morphology was examined by phase-contrast microscopic observation (E). Values shown are mean ± S.E.M. ($n = 3$). $^{\#}$ $P < 0.05$; ** or $^{\#\#}$ $P < 0.01$.

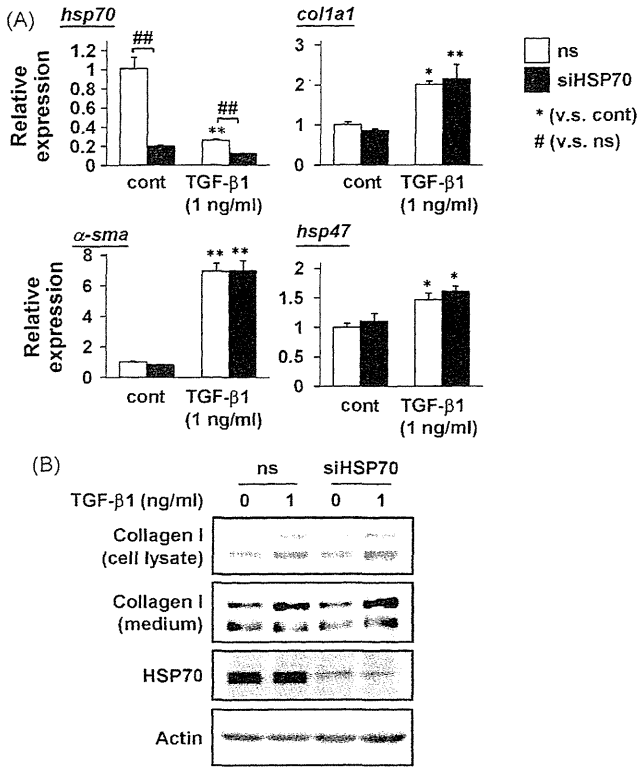

Fig. 6. Effect of siRNA for HSP70 on the TGF-β1-dependent activation of fibroblasts. HFL-I cells were transfected with 1.2 μg of siRNA for HSP70 (siHSP70) or non-silencing (ns) siRNA and incubated for 24 h. Cells were then incubated with the indicated concentrations of TGF-β1 for 24 h. Expression of each gene was examined by real-time RT-PCR as described in the legend of Fig. 4 (A). The levels of collagen I and HSP70 in cell lysate and collagen I in medium were examined by immunoblotting as described in the legend of Fig. 1 (B). Values shown are mean ± S.E.M. ($n = 3$). *$P < 0.05$; ** or ## $P < 0.01$.

Given that an increase in alveolar epithelial cell apoptosis has been observed in human IPF [44], the apoptotic process is believed to play an important role in the development of IPF. We here showed that bleomycin-induced pulmonary damage and epithelial cell apoptosis were suppressed in transgenic mice overexpressing HSP70. It is well known that HSP70 has anti-apoptotic effects through various mechanisms such as binding to apoptotic protease activating factor (Apaf)-1 to prevent the activation of caspase-9, suppression of the apoptotic pathway downstream of caspase-3 activation, and suppression of apoptosis-inducing factor-induced chromatin condensation [45–48]. We recently reported that HSP70 inhibits the activation of bcl-2-associated X protein (BAX), which is important for apoptosis-related mitochondrial dysfunction [32]. We consider that these mechanisms are involved in the HSP70-dependent suppression of bleomycin-induced lung epithelial cell apoptosis, because the activation of BAX and of caspases were reported to play an important role in bleomycin-induced apoptosis in lung epithelial cells [49,50].

In addition to this anti-apoptotic (cytoprotective) effect of HSP70, its anti-inflammatory effect was recently revealed and is thought to be important for its protective role against various diseases. HSP70 suppresses the activation of nuclear factor kappa B (NF-κB; an inflammation-inducing transcription factor) through various mechanisms such as suppression of inflammatory stimuli-induced degradation of IκB-a (an inhibitor of NF-κB) [18,51]. We previously reported that inflammatory responses (such as expression of pro-inflammatory cytokines and infiltration of leucocytes) in the stomach, colon and skin were suppressed in transgenic mice overexpressing HSP70 and that this suppression is mediated by the inhibition of NF-κB [23,32,34,35]. In this study, we showed that a bleomycin-induced increase in leucocytes in BALF and the pulmonary expression of pro-inflammatory cytokines were suppressed in transgenic mice overexpressing HSP70. We also showed that production of TGF-β1 was suppressed in bleomycin-treated transgenic mice overexpressing HSP70 compared to corresponding wild-type mice. This is the first demonstration of the inhibitory effect of HSP70 on the production of TGF-β1. It is known that TNF-α induces the expression of TGF-β1 [52] suggesting that the inhibitory effect of HSP70 on NF-κB and the resulting decrease in the level of TNF-α are responsible for this inhibitory effect of HSP70 on TGF-β1 production. Since TGF-β1 plays a major role in bleomycin-induced pulmonary fibrosis through various mechanisms such as activation of fibroblasts and stimulation of EMT of epithelial cells, the inhibitory effect of HSP70 on the production of TGF-β1 should be responsible for its protective effect against bleomycin-induced pulmonary fibrosis.

We also examined the effect of HSP70 expression on TGF-β1-dependent cellular responses involved in pulmonary fibrosis. We found that the TGF-β1-dependent induction of EMT-like phenotypes in lung epithelial cells (up-regulation of expression of markers of myofibroblasts and down-regulation of expression of markers of epithelial cells) and up-regulation of the expression of Slug (a transcription factor inducing EMT) were stimulated by the suppression of HSP70 expression. On the other hand, the TGF-β1-dependent activation of fibroblasts was not affected by the suppression of HSP70 expression. These results suggest that the expression of HSP70 suppresses the bleomycin-induced increase in lung myofibroblast number via suppression of the TGF-β1-dependent EMT of epithelial cells rather than via the activation of fibroblasts. It was recently reported that expression of HSP70 in cultured rat kidney proximal tubular epithelial cells inhibited TGF-β1-induced EMT, although the mechanism governing this inhibition is unknown [53]. Thus, it seems that expression of HSP70 generally suppresses EMT of epithelial cells. It is possible that the inhibitory effect of extracellular HSP70 on mitogen-activated protein kinases (MAPKs) [54] is involved in the inhibitory effect of HSP70 on the TGF-β1-induced EMT of epithelial cells, because MAPKs are involved in TGF-β1-dependent signal transduction pathways [55]. Furthermore, it is also possible that HSP70 achieves its inhibitory effect on EMT via the inhibition of NF-κB, because it was recently reported that NF-κB stimulates EMT via a mechanism that is independent on TGF-β1 [56].

While bleomycin-induced pulmonary fibrosis has been used as an animal model of IPF, this model does however has some limitations, such as the spontaneous resolution of fibrosis, which is rare in human IPF [57]. Furthermore, although assessment tools used in bleomycin-induced pulmonary fibrosis are primarily based on histology and quantitative collagen analysis, clinical management of IPF relies on lung function analysis. Therefore, in this study, we used a computer-controlled small-animal ventilator to monitor the bleomycin-induced decrease in compliance and increase in elastance, which are known to be associated with human IPF [58]. We found that these bleomycin-induced alterations in lung mechanics were ameliorated in transgenic mice overexpressing HSP70, suggesting that an increased expression of HSP70 could potentially improve the pulmonary dysfunction associated with human IPF.

As described above, it was recently reported that administration of GGA ameliorates bleomycin-induced pulmonary fibrosis [40], a result that we confirmed in this study. We also found that the administration of GGA improved lung function in the presence of bleomycin treatment. As described in Section 1, current agents for the treatment of IPF have not been found to improve the

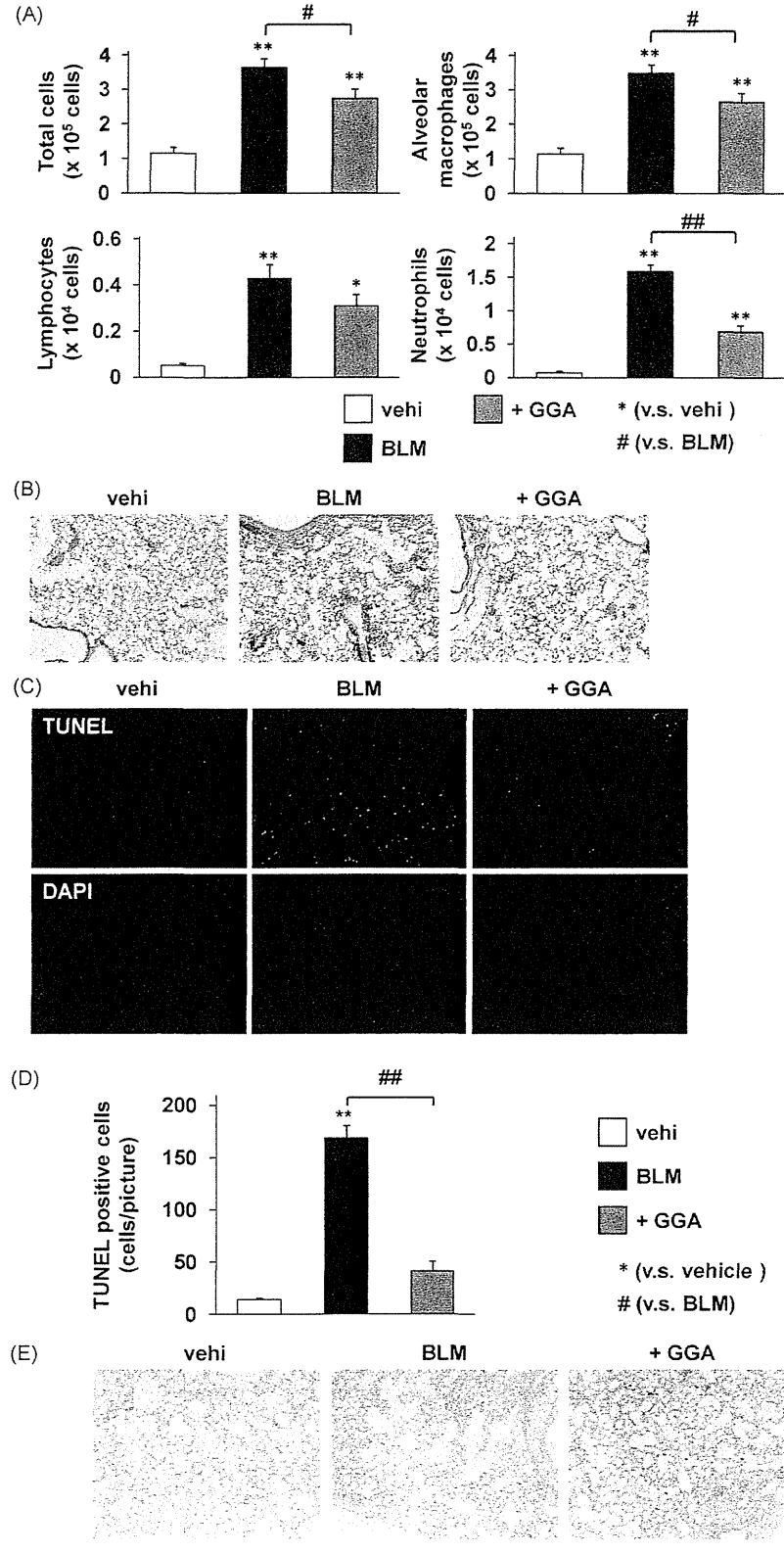

Fig. 7. Effect of oral administration of GGA on bleomycin-induced pulmonary damage, inflammatory response, fibrosis and dysfunction. C57/BL6 mice were orally administered with GGA (200 mg/kg) once per day for 3 days (A–E) or 14 days (F–H). Quercetin (200 mg/kg) was orally administered into mice 30 min before each administration of GGA (F–H). Mice were treated with (BLM) or without (vehi) bleomycin (5 mg/kg) once-only at day 0 and cells in BALF (A), pulmonary damage (B–D), pulmonary fibrosis (F and G) and lung mechanics (H) were assessed as described in the legends of Figs. 2 and 3. Immunohistochemical analysis with an antibody against HSP70 was performed as described in Section 2 (E). Values shown are mean ± S.E.M. ($n = 3$–12). *, # or $^{\$} < 0.05$; **, ## or $^{\$\$}P < 0.01$.

prognosis [1,3,4,59]. We consider that HSP70-inducers such as GGA could be beneficial for the prophylaxis of IPF. The development of new molecules as candidate drugs to treat this disease must pass through the clinical trials process and may encounter unanticipated side effects. Thus, based on the results of this study, we propose that clinical studies should be performed to prove the effectiveness of GGA for treating IPF given that the safety of GGA has already been shown clinically.

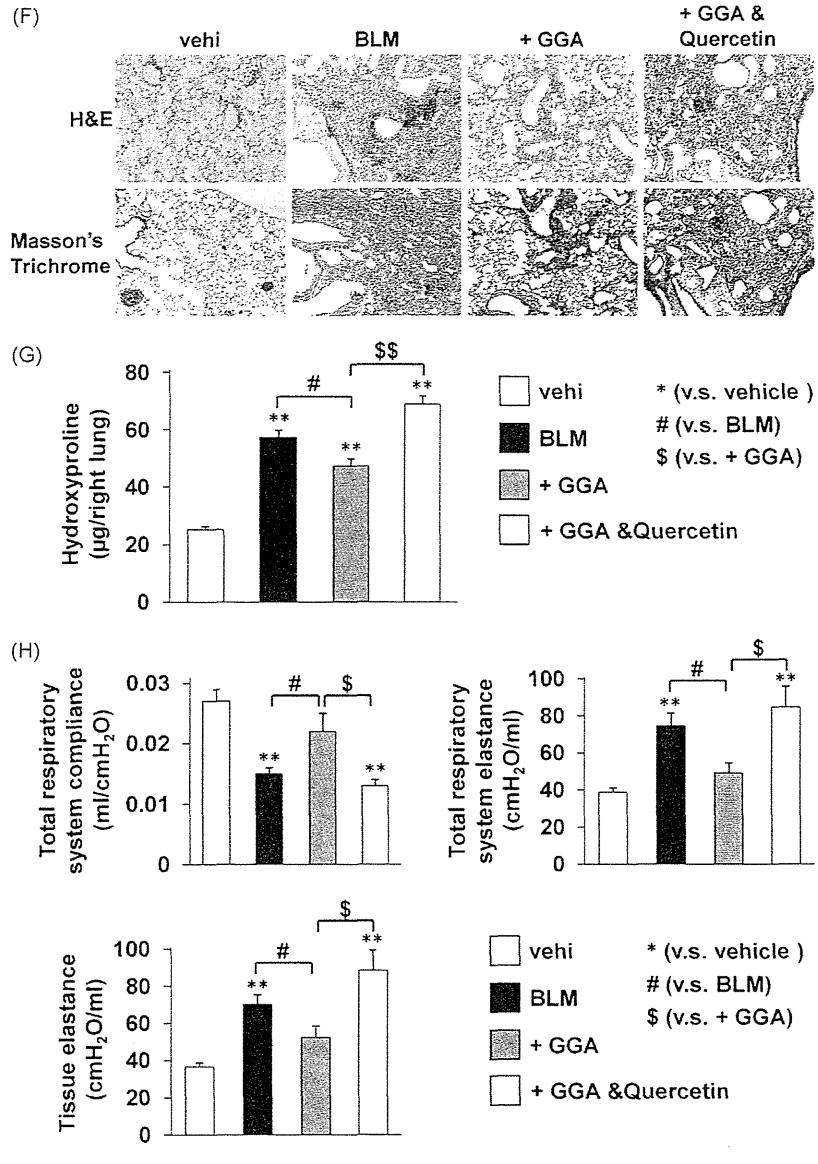

Fig. 7. (*Continued*).

Acknowledgements

This work was supported by Grants-in-Aid for Scientific Research from the Ministry of Health, Labour, and Welfare of Japan, as well as the Japan Science and Technology Agency and Grants-in-Aid for Scientific Research from the Ministry of Education, Culture, Sports, Science and Technology, Japan.

References

[1] American Thoracic Society. Idiopathic pulmonary fibrosis: diagnosis and treatment. International consensus statement. American Thoracic Society (ATS), and the European Respiratory Society (ERS). Am J Respir Crit Care Med 2000;161:646–64.
[2] Bjoraker JA, Ryu JH, Edwin MK, Myers JL, Tazelaar HD, Schroeder DR, et al. Prognostic significance of histopathologic subsets in idiopathic pulmonary fibrosis. Am J Respir Crit Care Med 1998;157:199–203.
[3] American Thoracic Society/European Respiratory Society International Multidisciplinary Consensus Classification of the Idiopathic Interstitial Pneumonias. This joint statement of the American Thoracic Society (ATS), and the European Respiratory Society (ERS) was adopted by the ATS board of directors, June 2001 and by the ERS Executive Committee, June 2001. Am J Respir Crit Care Med 2002;165:277–304.
[4] Walter N, Collard HR, King Jr TE. Current perspectives on the treatment of idiopathic pulmonary fibrosis. Proc Am Thorac Soc 2006;3:330–8.
[5] Moore BB, Hogaboam CM. Murine models of pulmonary fibrosis. Am J Physiol Lung Cell Mol Physiol 2008;294:L152–60.
[6] Kinnula VL, Myllarniemi M. Oxidant-antioxidant imbalance as a potential contributor to the progression of human pulmonary fibrosis. Antioxid Redox Signal 2008;10:727–38.
[7] Sheppard D. Transforming growth factor beta: a central modulator of pulmonary and airway inflammation and fibrosis. Proc Am Thorac Soc 2006;3:413–7.
[8] Kisseleva T, Brenner DA. Fibrogenesis of parenchymal organs. Proc Am Thorac Soc 2008;5:338–42.
[9] Willis BC, Borok Z. TGF-beta-induced EMT: mechanisms and implications for fibrotic lung disease. Am J Physiol Lung Cell Mol Physiol 2007;293:L525–34.
[10] Bartram U, Speer CP. The role of transforming growth factor beta in lung development and disease. Chest 2004;125:754–65.
[11] Kasai H, Allen JT, Mason RM, Kamimura T, Zhang Z. TGF-beta1 induces human alveolar epithelial to mesenchymal cell transition (EMT). Respir Res 2005;6:56.
[12] Kim KK, Kugler MC, Wolters PJ, Robillard L, Galvez MG, Brumwell AN, et al. Alveolar epithelial cell mesenchymal transition develops in vivo during pulmonary fibrosis and is regulated by the extracellular matrix. Proc Natl Acad Sci USA 2006;103:13180–5.
[13] Kim Y, Kugler MC, Wei Y, Kim KK, Li X, Brumwell AN, et al. Integrin alpha3beta1-dependent beta-catenin phosphorylation links epithelial Smad signaling to cell contacts. J Cell Biol 2009;184:309–22.
[14] Wu Z, Yang L, Cai L, Zhang M, Cheng X, Yang X, et al. Detection of epithelial to mesenchymal transition in airways of a bleomycin induced pulmonary fibrosis model derived from an alpha-smooth muscle actin-Cre transgenic mouse. Respir Res 2007;8:1.

[15] Kim KK, Wei Y, Szekeres C, Kugler MC, Wolters PJ, Hill ML, et al. Epithelial cell alpha3beta1 integrin links beta-catenin and Smad signaling to promote myofibroblast formation and pulmonary fibrosis. J Clin Invest 2009;119: 213–24.
[16] Mathew A, Morimoto RI. Role of the heat-shock response in the life and death of proteins. Ann N Y Acad Sci 1998;851:99–111.
[17] Hirakawa T, Rokutan K, Nikawa T, Kishi K. Geranylgeranylacetone induces heat shock proteins in cultured guinea pig gastric mucosal cells and rat gastric mucosa. Gastroenterology 1996;111:345–57.
[18] Tang D, Kang R, Xiao W, Wang H, Calderwood SK, Xiao X. The anti-inflammatory effects of heat shock protein 72 involve inhibition of high-mobility-group box 1 release and proinflammatory function in macrophages. J Immunol 2007;179:1236–44.
[19] Weiss YG, Maloyan A, Tazelaar J, Raj N, Deutschman CS. Adenoviral transfer of HSP-70 into pulmonary epithelium ameliorates experimental acute respiratory distress syndrome. J Clin Invest 2002;110:801–6.
[20] Koh Y, Lim CM, Kim MJ, Shim TS, Lee SD, Kim WS, et al. Heat shock response decreases endotoxin-induced acute lung injury in rats. Respirology 1999;4: 325–30.
[21] Hagiwara S, Iwasaka H, Matsumoto S, Noguchi T, Yoshioka H. Association between heat stress protein 70 induction and decreased pulmonary fibrosis in an animal model of acute lung injury. Lung 2007;185:287–93.
[22] Singleton KD, Wischmeyer PE. Effects of HSP70.1/3 gene knockout on acute respiratory distress syndrome and the inflammatory response following sepsis. Am J Physiol Lung Cell Mol Physiol 2006;290:L956–61.
[23] Tanaka K, Namba T, Arai Y, Fujimoto M, Adachi H, Sobue G, et al. Genetic evidence for a protective role for heat shock factor 1 and heat shock protein 70 against colitis. J Biol Chem 2007;282:23240–52.
[24] Woessner Jr JF. The determination of hydroxyproline in tissue and protein samples containing small proportions of this imino acid. Arch Biochem Biophys 1961;93:440–7.
[25] Mima S, Tsutsumi S, Ushijima H, Takeda M, Fukuda I, Yokomizo K, et al. Induction of claudin-4 by nonsteroidal anti-inflammatory drugs and its contribution to their chemopreventive effect. Cancer Res 2005;65:1868–76.
[26] Lovgren AK, Jania LA, Hartney JM, Parsons KK, Audoly LP, Fitzgerald GA, et al. COX-2-derived prostacyclin protects against bleomycin-induced pulmonary fibrosis. Am J Physiol Lung Cell Mol Physiol 2006;291:L144–56.
[27] Plumier JC, Ross BM, Currie RW, Angelidis CE, Kazlaris H, Kollias G, et al. Transgenic mice expressing the human heat shock protein 70 have improved post-ischemic myocardial recovery. J Clin Invest 1995;95:1854–60.
[28] Ishii H, Mukae H, Kakugawa T, Iwashita T, Kaida H, Fujii T, et al. Increased expression of collagen-binding heat shock protein 47 in murine bleomycin-induced pneumopathy. Am J Physiol Lung Cell Mol Physiol 2003;285:L957–63.
[29] Inoue K, Takano H, Yanagisawa R, Sakurai M, Abe S, Yoshino S, et al. Effects of nanoparticles on lung physiology in the presence or absence of antigen. Int J Immunopathol Pharmacol 2007;20:737–44.
[30] Peinado H, Olmeda D, Cano A. Snail, Zeb and bHLH factors in tumour progression: an alliance against the epithelial phenotype? Nat Rev Cancer 2007;7: 415–28.
[31] Thiery JP, Sleeman JP. Complex networks orchestrate epithelial–mesenchymal transitions. Nat Rev Mol Cell Biol 2006;7:131–42.
[32] Suemasu S, Tanaka K, Namba T, Ishihara T, Katsu T, Fujimoto M, et al. A role for HSP70 in protecting against indomethacin-induced gastric lesions. J Biol Chem 2009;284:19705–1.
[33] Tanaka K, Tsutsumi S, Arai Y, Hoshino T, Suzuki K, Takaki E, et al. Genetic evidence for a protective role of heat shock factor 1 against irritant-induced gastric lesions. Mol Pharmacol 2007;71:985–93.
[34] Asano T, Tanaka K, Yamakawa N, Adachi H, Sobue G, Goto H, et al. HSP70 confers protection against indomethacin-induced lesions of the small intestine. J Pharmacol Exp Ther 2009;330:458–67.
[35] Matsuda M, Hoshino T, Yamashita Y, Tanaka KI, Maji D, Sato K, et al. Prevention of ultraviolet B radiation-induced epidermal damage by expression of heat shock protein 70. J Biol Chem 2009.
[36] Gupte AA, Bomhoff GL, Swerdlow RH, Geiger PC. Heat treatment improves glucose tolerance and prevents skeletal muscle insulin resistance in rats fed a high-fat diet. Diabetes 2009;58:567–78.
[37] Katsuno M, Sang C, Adachi H, Minamiyama M, Waza M, Tanaka F, et al. Pharmacological induction of heat-shock proteins alleviates polyglutamine-mediated motor neuron disease. Proc Natl Acad Sci USA 2005;102:16801–6.
[38] Kuboki S, Schuster R, Blanchard J, Pritts TA, Wong HR, Lentsch AB. Role of heat shock protein 70 in hepatic ischemia-reperfusion injury in mice. Am J Physiol Gastrointest Liver Physiol 2007;292:G1141–9.
[39] Ohkawara T, Nishihira J, Takeda H, Miyashita K, Kato K, Kato M, et al. Geranylgeranylacetone protects mice from dextran sulfate sodium-induced colitis. Scand J Gastroenterol 2005;40:1049–57.
[40] Fujibayashi T, Hashimoto N, Jijiwa M, Hasegawa Y, Kojima T, Ishiguro N. Protective effect of geranylgeranylacetone, an inducer of heat shock protein 70, against drug-induced lung injury/fibrosis in an animal model. BMC Pulm Med 2009;9:45.
[41] Terano A, Hiraishi H, Ota S, Sugimoto T. Geranylgeranylacetone, a novel anti-ulcer drug, stimulates mucus synthesis and secretion in rat gastric cultured cells. Digestion 1986;33:206–10.
[42] Kunisaki C, Sugiyama M. Effect of teprenone on acute gastric mucosal lesions induced by cold-restraint stress. Digestion 1992;53:45–53.
[43] Ushijima H, Tanaka K, Takeda M, Katsu T, Mima S, Mizushima T. Geranylgeranylacetone protects membranes against nonsteroidal anti-inflammatory drugs. Mol Pharmacol 2005;68:1156–61.
[44] Thannickal VJ, Horowitz JC. Evolving concepts of apoptosis in idiopathic pulmonary fibrosis. Proc Am Thorac Soc 2006;3:350–6.
[45] Saleh A, Srinivasula SM, Balkir L, Robbins PD, Alnemri ES. Negative regulation of the Apaf-1 apoptosome by Hsp70. Nat Cell Biol 2000;2:476–83.
[46] Beere HM, Wolf BB, Cain K, Mosser DD, Mahboubi A, Kuwana T, et al. Heat-shock protein 70 inhibits apoptosis by preventing recruitment of procaspase-9 to the Apaf-1 apoptosome. Nat Cell Biol 2000;2:469–75.
[47] Ravagnan L, Gurbuxani S, Susin SA, Maisse C, Daugas E, Zamzami N, et al. Heat-shock protein 70 antagonizes apoptosis-inducing factor. Nat Cell Biol 2001;3: 839–43.
[48] Jaattela M, Wissing D, Kokholm K, Kallunki T, Egeblad M. Hsp70 exerts its anti-apoptotic function downstream of caspase-3-like proteases. EMBO J 1998;17: 6124–34.
[49] Li X, Zhang H, Soledad-Conrad V, Zhuang J, Uhal BD. Bleomycin-induced apoptosis of alveolar epithelial cells requires angiotensin synthesis de novo. Am J Physiol Lung Cell Mol Physiol 2003;284:L501–7.
[50] Lee VY, Schroedl C, Brunelle JK, Buccellato LJ, Akinci OI, Kaneto H, et al. Bleomycin induces alveolar epithelial cell death through JNK-dependent activation of the mitochondrial death pathway. Am J Physiol Lung Cell Mol Physiol 2005;289:L521–8.
[51] Weiss YG, Bromberg Z, Raj N, Raphael J, Goloubinoff P, Ben-Neriah Y, et al. Enhanced heat shock protein 70 expression alters proteasomal degradation of IkappaB kinase in experimental acute respiratory distress syndrome. Crit Care Med 2007;35:2128–38.
[52] Sullivan DE, Ferris M, Pociask D, Brody AR. The latent form of TGFbeta(1) is induced by TNFalpha through an ERK specific pathway and is activated by asbestos-derived reactive oxygen species in vitro and in vivo. J Immunotoxicol 2008;5:145–9.
[53] Mao H, Li Z, Zhou Y, Zhuang S, An X, Zhang B, et al. HSP72 attenuates renal tubular cell apoptosis and interstitial fibrosis in obstructive nephropathy. Am J Physiol Renal Physiol 2008;295:F202–14.
[54] Luo X, Zuo X, Zhou Y, Zhang B, Shi Y, Liu M, et al. Extracellular heat shock protein 70 inhibits tumour necrosis factor-alpha induced proinflammatory mediator production in fibroblast-like synoviocytes. Arthritis Res Ther 2008;10:R41.
[55] He S, Liu X, Yang Y, Huang W, Xu S, Yang S, et al. Mechanisms of transforming growth factor beta/Smad signalling mediated by mitogen-activated protein kinase pathways in keloid fibroblasts. Br J Dermatol 2009.
[56] Huber MA, Azoitei N, Baumann B, Grunert S, Sommer A, Pehamberger H, et al. NF-kappaB is essential for epithelial–mesenchymal transition and metastasis in a model of breast cancer progression. J Clin Invest 2004;114: 569–81.
[57] Moeller A, Ask K, Warburton D, Gauldie J, Kolb M. The bleomycin animal model: a useful tool to investigate treatment options for idiopathic pulmonary fibrosis? Int J Biochem Cell Biol 2008;40:362–82.
[58] Ask K, Labiris R, Farkas L, Moeller A, Froese A, Farncombe T, et al. Comparison between conventional and "clinical" assessment of experimental lung fibrosis. J Transl Med 2008;6:16.
[59] Luppi F, Cerri S, Beghe B, Fabbri LM, Richeldi L. Corticosteroid and immunomodulatory agents in idiopathic pulmonary fibrosis. Respir Med 2004;98: 1035–44.

THE JOURNAL OF BIOLOGICAL CHEMISTRY VOL. 285, NO. 48, pp. 37302–37313, November 26, 2010

Suppression of Expression of Endoplasmic Reticulum Chaperones by *Helicobacter pylori* and Its Role in Exacerbation of Non-steroidal Anti-inflammatory Drug-induced Gastric Lesions*[S]

Received for publication, May 26, 2010, and in revised form, September 21, 2010 Published, JBC Papers in Press, September 22, 2010, DOI 10.1074/jbc.M110.148882

Takushi Namba[‡], Tatsuya Hoshino[‡], Shintaro Suemasu[‡], Mika Takarada-Iemata[§], Osamu Hori[§], Naomi Nakagata[¶], Akinori Yanaka[‖], and Tohru Mizushima[‡1]

From the [‡]Graduate School of Medical and Pharmaceutical Sciences, Kumamoto University, Kumamoto 862-0973, the [§]Department of Neuroanatomy, Kanazawa University Graduate School of Medical Science, Kanazawa 920-8640, the [¶]Center for Animal Resources and Development, Institute of Resource Development and Analysis, Kumamoto University, Kumamoto 860-0811, and the [‖]Division of Clinical Pharmacology, Faculty of Pharmaceutical Sciences, Tokyo University of Science, Noda 278-8510, Japan

Both the use of non-steroidal anti-inflammatory drugs (NSAIDs), such as indomethacin, and infection with *Helicobacter pylori* are major causes of gastric ulcers. Although some clinical studies suggest that infection with *H. pylori* increases the risk of developing NSAID-induced gastric lesions, the molecular mechanism governing this effect is unknown. We recently found that in cultured gastric cells, expression of endoplasmic reticulum (ER) chaperones (such as 150-kDa oxygen-regulated protein (ORP150) and glucose-regulated protein 78 (GRP78)) is induced by NSAIDs and confers protection against NSAID-induced apoptosis, which is important in the development of NSAID-induced gastric lesions. In this study we have found that co-culture of gastric cells with *H. pylori* suppresses the expression of ER chaperones. This suppression was regulated at the level of transcription and accompanied by a reduction in the level of activating transcription factor 6 (ATF6), one of the transcription factors for ER chaperone genes. *In vivo*, inoculation of mice with *H. pylori* suppressed the expression of ER chaperones at gastric mucosa both with and without administration of indomethacin. Inoculation with *H. pylori* also stimulated formation of indomethacin-induced gastric lesions and mucosal cell death. In addition, we found that heterozygous ORP150-deficient mice are sensitive to the development of indomethacin-induced gastric lesions and mucosal cell death. The results of this study suggest that *H. pylori* exacerbates NSAID-induced gastric lesions through suppression of expression of ER chaperones, which stimulates NSAID-induced mucosal cell death.

The balance between aggressive and defensive factors determines whether gastric ulcers develop. The gastric mucosa is challenged by a variety of aggressive factors, and of these, both non-steroidal anti-inflammatory drugs (NSAIDs)[2] and *Helicobacter pylori* are major causes of gastric lesions. Therefore, an important question is whether infection with *H. pylori* increases the risk of developing NSAID-induced gastric lesions (in other words, if eradication of *H. pylori* would reduce the risk of developing NSAID-induced gastric lesions). Recent clinical studies suggest that infection with *H. pylori* increases the risk of developing NSAID-induced gastric lesions (1–4); however, some studies have shown the opposite effect (5, 6). Animal models could be useful to address this issue. For example, some reports have demonstrated that NSAID-induced gastric lesions in mongolian gerbils are exacerbated by infection with *H. pylori* (7–9), although the molecular mechanism governing this exacerbation is unclear.

An inhibitory effect of NSAIDs on cyclooxygenase (COX) activity and the resulting decrease in the gastric level of prostaglandins (PGs), especially PGE_2, was believed to be the only explanation for the gastric side effects of NSAIDs because PGE_2 is a strong protective factor for gastric mucosa (10). However, the increased incidence of gastrointestinal lesions and the decrease in PG levels induced by NSAIDs are not always linked with each other. For example, it has been shown that higher doses of NSAIDs are required for producing gastric lesions than are required for inhibiting COX at the gastric mucosa (11), suggesting that there are additional mechanisms involved in the development of NSAID-induced gastric lesions. We have recently demonstrated that NSAIDs induce apoptosis in cultured gastric mucosal cells and at gastric mucosa in a manner independent of COX inhibition (12–16) and have suggested that both COX inhibition (measured as a decrease in the gastric PGE_2 level) and gastric mucosal apoptosis are required for the formation of NSAID-induced gastric lesions (16–18). There-

* This work was supported by grants-in-aid of Scientific Research from the Ministry of Health, Labour, and Welfare of Japan, grants-in-aid for Scientific Research from the Ministry of Education, Culture, Sports, Science, and Technology of Japan, and grants-in-aid of the Japan Science and Technology Agency.

[S] The on-line version of this article (available at http://www.jbc.org) contains supplemental Figs. S1–S5.

[1] To whom correspondence should be addressed. Tel.: and Fax: 81-96-371-4323; E-mail: mizu@gpo.kumamoto-u.ac.jp.

[2] The abbreviations used are: NSAID, non-steroidal anti-inflammatory drug; ATF, activating transcription factor; CagA, cytotoxin-associated gene A; CHOP, C/EBP homologous transcription factor; ER, endoplasmic reticulum; ERSE, ER stress response element; GRP78, glucose-regulated protein 78; IRE1, protein-kinase and site-specific endoribonuclease; PERK, protein kinase R-like ER kinase; ORP150, 150-kDa oxygen-regulated protein; PG, prostaglandin; S1P, site-1 protease; S2P, site-2 protease; VacA, vacuolating cytotoxin A; XBP, X box binding protein.

fore, protection against gastric mucosal apoptosis is important for protecting gastric mucosa against the formation of NSAID-induced lesions. As for the molecular mechanism governing this apoptosis, we have proposed the following pathway. Permeabilization of cytoplasmic membranes by NSAIDs stimulates Ca^{2+} influx and increases intracellular Ca^{2+} levels, which in turn induces the endoplasmic reticulum (ER) stress response (12, 13, 19, 20). In the ER stress response, an apoptosis-inducing transcription factor, C/EBP homologous transcription factor (CHOP), is induced. We have previously shown that CHOP is essential for NSAID-induced apoptosis (13). CHOP induces expression of p53 up-regulated modulator of apoptosis and the resulting activation of Bax, mitochondrial dysfunction, and the activation of caspases and apoptosis (18, 21).

The ER stress response is induced by accumulation of unfolded proteins in the ER, a process involving three types of ER transmembrane proteins: protein kinase and site-specific endoribonuclease (IRE1), protein kinase R-like ER kinase (PERK), and activating transcription factor 6 (ATF6) (22–24). ER stressors phosphorylate PERK, which in turn phosphorylates eukaryotic initiation factor-2α, leading to the activation of ATF4 expression (25). In the presence of ER stressors, p90-ATF6 (full-length ATF6) is translocated from the ER to the Golgi apparatus, where it is sequentially cleaved by site-1 protease (S1P) and site-2 protease (S2P) into p50-ATF6 (24). Activation of IRE1 causes frame switch splicing of X box-binding protein 1 (XBP-1), which produces the active (spliced) form of XBP-1 (26). All of ATF4, p50-ATF6, and XBP-1 specifically activate the transcription of ER stress response-related genes. ER stress response-related proteins contain not only CHOP but also ER chaperones (such as 150-kDa oxygen-regulated protein (ORP150) and glucose-regulated protein 78 (GRP78)) that confer protection against ER stressors by refolding unfolded proteins in the ER. We have recently reported that up-regulation of expression of GRP78 and ORTP150 by NSAIDs protects gastric cells from NSAID-induced apoptosis *in vitro* (19, 20), suggesting that ER chaperones are defensive factors for gastric mucosa. Although it has been reported that expression of ER chaperones is induced with the development of gastric lesions by water-immersion stress (27), there is no direct (such as genetic) evidence supporting the notion that ER chaperones are defensive factors for gastric mucosa.

The identification of *H. pylori* in the human stomach has changed the diagnosis and treatment of gastric diseases because it is now clear that *H. pylori* plays an important role in various gastric diseases, such as chronic gastritis, peptic ulcers, and gastric cancers (28, 29). This idea is supported by clinical results that eradication of *H. pylori* significantly decreases the risk of these gastric diseases (2, 30, 31). Infection with *H. pylori* damages gastric mucosa through production of ammonia and cytotoxic proteins such as vacuolating cytotoxin A (VacA) and cytotoxin-associated gene A (CagA) and induction of host inflammatory responses (32–36). In addition to these mechanisms, it is also possible that *H. pylori* damages gastric mucosa through decreasing the expression of host defensive factors for gastric mucosa. It was recently reported that *H. pylori* inhibit the expression of heat shock proteins and mucin, both of which are major defensive factors for gastric mucosa (35, 37). However, the effect of *H. pylori* on other defensive factors, including ER chaperones, has not been tested. In this study we found that co-culture of gastric cells with *H. pylori in vitro* decreases the expression of ER chaperones, and we suggest that this suppression is mediated by the degradation of ATF6. We also show that inoculation of mice with *H. pylori* not only suppresses the expression of ER chaperones at gastric mucosa but also exacerbates NSAID-induced gastric lesions and mucosal cell death. We have also found that heterozygous ORP150-deficient mice are sensitive to the development of NSAID-induced gastric lesions and mucosal cell death. The results of this study suggest that *H. pylori* exacerbates NSAID-induced gastric lesions through suppression of expression of ER chaperones and the resulting stimulation of NSAID-induced mucosal cell death.

EXPERIMENTAL PROCEDURES

Chemicals and Animals—RPMI 1640 and *Helicobacter* selection agar were obtained from Nissui Pharmaceutical Co (Osaka, Japan). Aneropack Bikouki was from Mitsubishi Gas Chemical (Tokyo, Japan). Horse serum was from Invitrogen. Paraformaldehyde, epoxomycin, cycloheximide, pepstatin A, and fetal bovine serum (FBS) were from Sigma. E-64-d was from the Peptide Institute Inc. (Tokyo, Japan). Indomethacin was obtained from Wako Co. (Osaka, Japan). Brain heart infusion was from Difco. Antibodies against GRP78, ATF4, ATF6, actin, lamin, the N-terminal region of Bax (Bax N20), and CHOP were from Santa Cruz Biotechnology (Santa Cruz, CA). Antibodies against GRP94, GRP58, and protein disulfide isomerase were from StressGen (San Diego, CA). An antibody against cytochrome *c* was from BD Biosciences, and that against connexin 43 was from Invitrogen. An antibody against GFP was from Clontech (Mountain View CA), and that against ORP150 was from our laboratory stocks (38). Terminal deoxynucleotidyltransferase was obtained from TOYOBO (Osaka, Japan). Biotin 14-ATP, Alexa Fluor 488 goat anti-rabbit (or anti-mice) immunoglobulin G, Alexa Fluor 594 goat anti-rat immunoglobulin G, Lipofectamine (TM2000), Dynabeads Protein G, and Alexa Fluor 488 conjugated with streptavidin were purchased from Invitrogen. Mounting medium for immunohistochemical analysis (VECTASHIELD) was from Vector Laboratories (Burlingame, CA). 4′,6-diamidino-2-phenylindole dihydrochloride (DAPI) was from Dojindo (Kumamoto, Japan). The RNeasy kit and HiPerFect transfection reagents were obtained from Qiagen (Valencia, CA), the first-strand cDNA synthesis kit was from Takara (Kyoto, Japan), and the iQ SYBR Green Supermix was from Bio-Rad. The Dual Luciferase Assay System was from Promega (Southampton, UK). Mice heterozygous for a truncated/inactivated mutant form of ORP150 ($ORP150^{+/-}$) and their wild-type counterparts ($ORP150^{+/+}$) (6–8 weeks of age) were prepared as described previously (38, 39). The experiments and procedures described here were carried out in accordance with the Guide for the Care and Use of Laboratory Animals as adopted and promulgated by the National Institutes of Health (Bethesda, MD) and were approved by the Animal Care Committee of Kumamoto University.

H. pylori Inoculation and Gastric Damage Assay—*H. pylori* inoculation was done as described previously (40) with some modifications. *H. pylori* strain ATCC43504 ($CagA^+$ and

VacA$^+$) (a gift from Dr. Oguma, Okayama University) was cultured in a brain heart infusion broth containing 10% horse serum at 37 °C under a microaerophilic atmosphere. *H. pylori* were also cultured on brain heart infusion agar supplemented with heat-inactivated 7% horse blood or on *Helicobacter* selection agar under a gas-pack jar with an Anaeropack Bikouki. Mice were orally inoculated with *H. pylori* at a dose of 2.0×10^8 *H. pylori*/animal/0.5 ml of PBS every second day for 6 days (total 3 times). *H. pylori* lysates were prepared by sonication of cells in PBS. The protein concentration of lysates was determined by the Bradford method (41).

The gastric ulcerogenic response was examined as described previously (18), with some modifications. *H. pylori*-inoculated or non-inoculated mice (1 day after the final inoculation of *H. pylori*) fasted for 6 h were orally administered with indomethacin (10 mg/kg, 10 ml 1% methylcellulose/kg). Twelve hours later, the animals were sacrificed, after which their stomachs were removed, and the areas of gastric mucosal lesions were measured by an observer unaware of the treatment they had received. Calculation of the scores involved measuring the area of all the lesions in square millimeters and summing the values to give an overall gastric lesion index.

Cell Culture—AGS and MKN45 are human adenocarcinoma gastric cell lines. Cells were cultured in RPMI1640 medium supplemented with 10% FBS, 100 units/ml penicillin, and 100 μg/ml streptomycin in a humidified atmosphere of 95% air with 5% CO_2 at 37 °C.

Transfections were carried out using Lipofectamine (TM2000) according to the manufacturer's instructions. Cells were used for experiments after a 24-h recovery period. Transfection efficiency was determined in parallel plates by transfection of cells with a pEGFP-N1 control vector. Transfection efficiencies were greater than 80% in all experiments. The plasmid pCMVshort-EGFP-ATF6α (a gift from Dr. Mori, Kyoto University) (42) was transfected into AGS cells, according to the manufacturer's protocols.

siRNA Targeting of Genes—The siRNAs for ATF6 and ATF4 and nonspecific siRNA were purchased from Qiagen. AGS cells were transfected with siRNA using HiPerFect transfection reagent according to the manufacturer's instructions.

Pulse-Chase Analysis—A pulse-chase experiment was carried out with 0.1 mCi/ml Expre^{35}S^{35}S protein labeling mix (PerkinElmer Life Sciences) as described previously (43), with some modifications. Cells were labeled with [^{35}S]methionine and [^{35}S]cysteine in methionine- and cysteine-free RPMI1640 medium for 30 min. To chase labeled proteins, cells were washed with fresh complete medium three times and incubated in fresh complete medium with or without *H. pylori*. ATF6 was immunoprecipitated with its antibody and separated by SDS-polyacrylamide gel electrophoresis followed by autoradiography (Fuji BAS 2500 imaging analyzer).

Immunostaining—Plasmids (pCMVshort-EGFP-ATF6α) were transfected into AGS cells, and cells were co-cultured with *H. pylori* in the Lab-Tek II chamber slide system (Nalge Nunc International, Rochester, NY). Cells were fixed in 4% paraformaldehyde for 20 min, blocked with goat serum for 15 min, then incubated for 12 h with antibody against GRP94 in the presence of 2.5% bovine serum albumin before finally being incubated for 2 h with Alexa Fluor 594 goat anti-rat IgG. Samples were mounted with VECTASHIELD. Images were captured on a confocal laser-scanning fluorescence microscope (FLUOVIEW FV500-IX-UV, Olympus).

RT-PCR and Real-time RT-PCR Analyses—Real-time RT-PCR was performed as previously described with some modifications (44). Total RNA was extracted from gastric tissues or cultured cells using an RNeasy kit according to the manufacturer's protocol. Samples (2.5 μg RNA) were reverse-transcribed using a first-strand cDNA synthesis kit. Synthesized cDNA was used in real-time RT-PCR (Chromo 4 instrument; Bio-Rad) experiments using iQ SYBR GREEN Supermix and analyzed with Opticon Monitor Software. Specificity was confirmed by electrophoretic analysis of the reaction products and by the inclusion of template- or reverse transcriptase-free controls. The cycle conditions were 2 min at 50 °C followed by 10 min at 90 °C and finally 45 cycles of 95 °C for 30 s and 63 °C for 60 s. To normalize the amount of total RNA present in each reaction, actin cDNA was used as an internal standard.

Primers were designed using the Primer3 website and are listed as forward and reverse, respectively. Human primers were: *atf4* (5′-tcaaacctcatgggttctcc-3′) and (5′-gtgtcatccaacgtggtcag-3′); *atf6*, (5′-ctccgagatcagcagaggaa-3′) and (5′-aatgactcagggatggtgct-3′); *chop*, (5′-tgcctttctcttcggacact-3′) and (5′-tgtgacctctgctggttctg-3′); *grp78*, (5′-tagcgtatggtgctgctgtc-3′) and (5′-tttgtcaggggtctttcacc-3′); *orp150*, (5′-gaagatgcagagcccatttc-3′) and (5′-tctgctccaggacctcctaa-3′); *xbp-1*, (5′-aaacagagtagcagcgcagactg-3′) and (5′-ggatctctaaaactagaggcttggtg-3′); *xbp-1 (u)*, (5′-agcactcagactacgtgcac-3′) and (5′-ccagaatgcccaacaggata-3′); actin, (5′-ggacttcgagcaagagatgg-3′) and (5′- agcactgtgttggcgtacag-3′). Mouse primers were: *atf6* (5′-catcaaaagctcctcggttc-3′) and (5′-gggtcgtctctgtggttgtt-3′); *grp78*, (5′-gcttccgataatcagccaac-3′) and (5′-gcaggaggaattccagtca-3′); *orp150*, (5′-cagactgaagaggcgaaacc-3′) and (5′-ttcctgttcaggtccagctc-3′); *chop*, (5′-acagaggtcacacgcacatc-3′), and (5′-gggcactgaccactctgttt-3′); *gapdh*, (5′-tgcctttctcttcggacact-3′ and (5′-tgtgacctctgctggttctg-3′).

For regular RT-PCR, we used an initial denaturation step of 94 °C for 1 min followed by 30 cycles of denaturation at 94 °C for 30 s, annealing at 60 °C for 20 s, and elongation at 72 °C for 1 min. A final elongation step at 72 °C for 10 min completed the RT-PCR. The amplified PCR products were separated by 3% agarose gel electrophoresis and then visualized with ethidium bromide.

Immunoblotting Analysis—Total protein and nuclear protein extracts were prepared as described previously (20). The protein concentration of each sample was determined by the Bradford method (41). Samples were applied to polyacrylamide SDS gels and subjected to electrophoresis, after which the proteins were immunoblotted with appropriate antibodies.

Histological, Immunohistochemical, and Terminal Deoxynucleotidyltransferase-mediated Biotinylated UTP Nick End Labeling (TUNEL) Analyses—Gastric tissue samples were fixed in 4% buffered paraformaldehyde and embedded in paraffin before being cut into 4-mm sections.

For histological examination (hematoxylin and eosin (H&E) staining), sections were stained first with Mayer's hematoxylin and then with 1% eosin alcohol solution. Samples were

mounted with Malinol and inspected with the aid of an Olympus BX51 microscope.

For immunohistochemical analysis, sections were blocked with 2.5% goat serum for 10 min, incubated for 12 h with antibody against ORP150 or GRP78 in the presence of 2.5% bovine serum albumin, and finally incubated for 2 h with Alexa Fluor 488 goat anti-rabbit immunoglobulin G in the presence of DAPI (5 mg/ml). Samples were mounted with VECTASHIELD and inspected using fluorescence microscopy (Olympus BX51).

For TUNEL assays, sections were incubated first with proteinase K (20 mg/ml) for 15 min at 37 °C, then with terminal deoxynucleotidyltransferase and biotin 14-ATP for 1 h at 37 °C and finally with Alexa Fluor 488 conjugated with streptavidin for 1 h. Samples were mounted with VECTASHIELD and inspected using fluorescence microscopy (Olympus BX51).

Luciferase Assay—The pGL-3/ERSE (ER stress response element) plasmid, which was constructed by inserting ERSE (5′-ccaatcagaaagtggcacg-3′) just upstream of the luciferase gene (45), was kindly provided by Dr. Gotoh (Kumamoto University). The pGL-3/*grp78*pro plasmid, which was constructed by inserting the human *grp78* promoter (from −304 to +7 region) into the same region (46), was generously provided by Dr. Mori (Kyoto University).

The luciferase assay was performed as described previously (47). Cells were transfected with 1 μg of one of the *Photinus pyralis* luciferase reporter plasmids (pGL-3 or its derivatives) and 0.125 μg of the internal standard plasmid bearing the *Renilla reniformis* luciferase reporter (pRL-SV40). *P. pyralis* luciferase activity in cell extracts was measured using the Dual Luciferase Assay System and then normalized for *R. reniformis* luciferase activity.

Statistical Analysis—Two-way analysis of variance followed by the Tukey test or the Student's *t* test for unpaired results was used to evaluate differences between more than three groups or between two groups, respectively. Differences were considered to be significant for values of $p < 0.05$.

RESULTS

Effect of H. pylori on Expression of ER Chaperones in Vitro—It was previously reported that co-culture of AGS cells with *H. pylori* at a bacteria:cell ratio of 200:1 causes partial induction of apoptosis (48, 49). In the current study we examined the expression of ER chaperones under these conditions and, using MTT (3-(4,5-dimethylthiazol-2-yl)-2,5-diphenyl tetrazolium bromide) assay, determined cell viability to be 80% after a 24-h incubation of AGS cells with *H. pylori* (data not shown). As shown in Fig. 1, *A* and *B*, treatment of cells with *H. pylori* decreased the levels of ORP150 and GRP78. Similar results were observed in another gastric cell line (MKN45) (Fig. 1*C*). A slight reduction of levels of other ER chaperones (such as GRP94 and protein disulfide isomerase but not GRP58) was also observed in cells treated with *H. pylori* (Fig. 1, *A* and *B*). We also found that treatment of AGS cells with *H. pylori* cell lysates also decreased the levels of ORP150 and GRP78; however, the extent of these decreases was not as apparent as that observed with *H. pylori* (Fig. 1, *D* and *E*). Unlike the ER chaperones, the level of CHOP was increased by co-culture of cells with *H. pylori* (Fig. 1, *A* and *B*).

Real-time RT-PCR analysis revealed that the *H. pylori*-dependent down-regulation of expression of ORP150 and GRP78 and up-regulation of expression of CHOP was also observed at the level of mRNA (Fig. 2*A*). We also performed a luciferase reporter assay using a reporter plasmid where the promoter of the *grp78* gene was inserted upstream of the luciferase gene (pGL-3/*grp78*pro). As shown in Fig. 2*B*, co-culture of cells with *H. pylori* decreased the luciferase activity in cells with pGL-3/*grp78*pro but not in those with the control vector (pGL-3). These results suggest that co-culture of cells with *H. pylori* inhibits the transcription of ER chaperone genes.

Mechanism for Suppression of Expression of ER Chaperones by H. pylori—To understand the molecular mechanism governing suppression of expression of ER chaperones by *H. pylori*, we first examined the effect of *H. pylori* on the level of ER stress response-related transcription factors (ATF6, ATF4, and XBP-1). Co-culture of cells with *H. pylori* decreased the level of ATF6 protein (p90-ATF6) but not *atf6* mRNA (Figs. 1, *A* and *B*, and 2*C*). We also found that the level of p50-ATF6 in nuclear extracts decreased after co-culture of cells with *H. pylori* (Fig. 1, *F* and *G*). On the other hand, the levels of ATF4 protein and *atf4* mRNA did not alter after co-culture with *H. pylori* (Figs. 1, *A* and *B*, and 2*C*). Furthermore, although treatment of cells with indomethacin increased the level of the spliced form (active form) of *xbp-1* mRNA, treatment of cells with *H. pylori* did not result in a similar observation (Fig. 2*D*). We also found that treatment of cells with indomethacin or *H. pylori* decreases or increases, respectively, the level of un-spliced form (inactive form) of *xbp-1* mRNA by real-time RT-PCR analysis (Fig. 2*E*). These results suggest that ATF6, rather than ATF4 and XBP-1, is responsible for suppression of expression of ER chaperones by *H. pylori*.

To confirm this idea, we performed a luciferase assay using a reporter plasmid where the ATF6 binding consensus sequence, ERSE, was inserted upstream of the luciferase gene (pGL-3/ERSE). As shown in Fig. 2*B*, treatment of cells with *H. pylori* decreased the luciferase activity in cells with pGL-3/ERSE, suggesting that the transcriptional activity of ATF6 decreased after treatment of cells with *H. pylori*. This is consistent with the observation that the level of p50-ATF6 decreased in *H. pylori*-treated cells (Fig. 1, *F* and *G*).

For further confirmation of the idea that ATF6 plays an important role in *H. pylori*-dependent suppression of expression of ER chaperones, we examined the effect of siRNA for ATF6 on the expression of ER chaperones. As shown in Fig. 3, transfection of cells with siRNA for ATF6 suppressed expression of not only ATF6 but also ORP150 and GRP78, affecting both mRNA and protein levels. The transfection did not affect the expression of *chop* mRNA (Fig. 3*A*). On the other hand, transfection of cells with siRNA for ATF4 suppressed expression of ATF4 but not that of ORP150 and GRP78 (supplemental Fig. S1). The results in Fig. 3 suggest that the reduction in the level of ATF6 is partly involved in the *H. pylori*-dependent suppression of expression of ER chaperones but not for induction of expression of CHOP.

We also examined the effect of *H. pylori* cell lysates on levels of p90-ATF6 and p50-ATF6. As shown in Fig. 1, *D*–*G*, levels of p90-ATF6 and p50-ATF6 were slightly decreased by

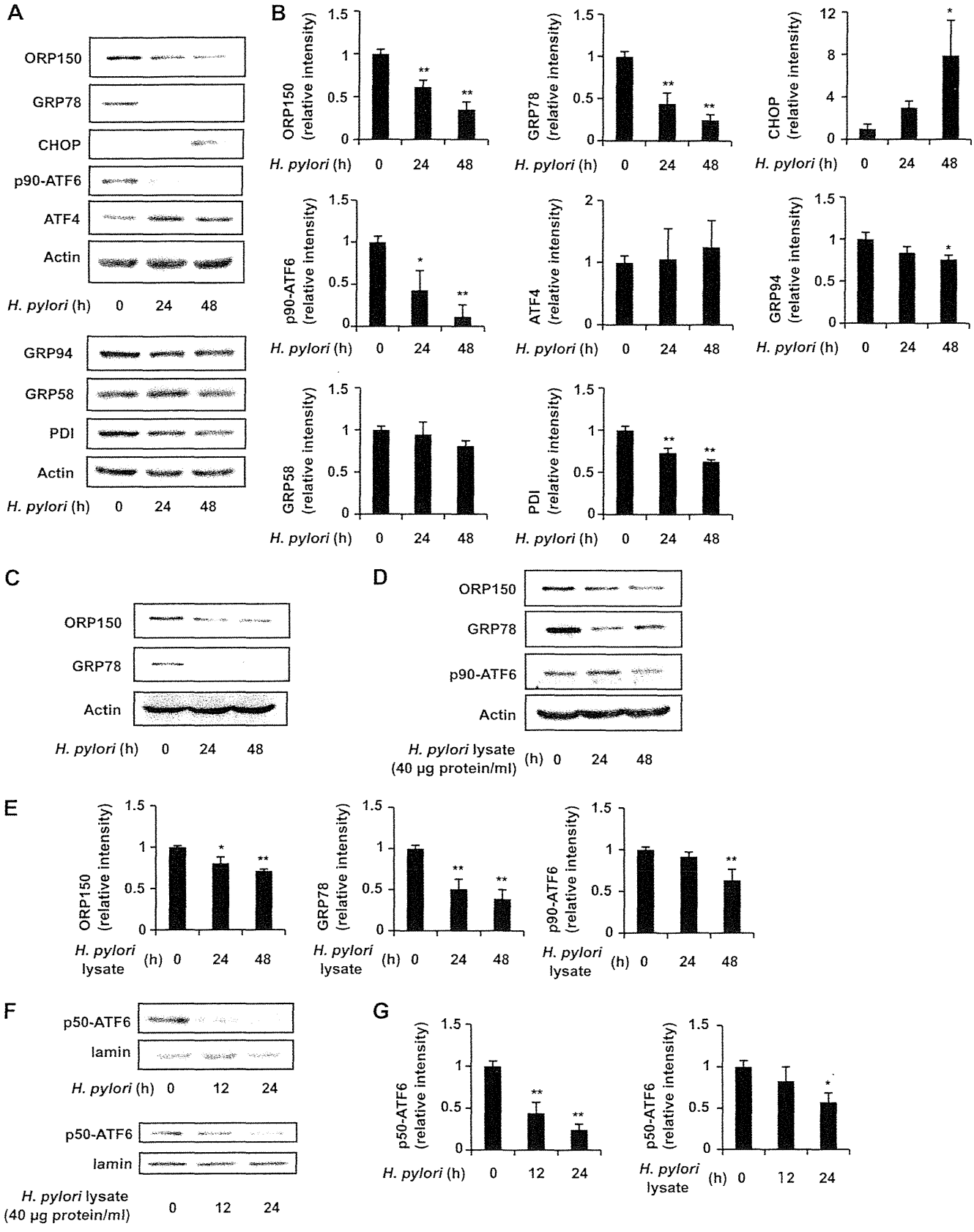

FIGURE 1. **Down-regulation of expression of ER chaperones by *H. pylori*.** AGS (*A*, *B*, and *D–G*) or MKN-45 (*C*) cells were co-cultured with *H. pylori* at a bacteria:cell ratio of 200:1 (*A–C*, *F*, and *G*) or with *H. pylori* lysates (*D–G*) for the indicated periods. Whole cell extracts (*A*, *C*, and *D*) or nuclear extracts (*F*) were analyzed by immunoblotting with an antibody against ORP150, GRP78, CHOP, ATF6, ATF4, GRP94, GRP58, protein disulfide isomerase (*PDI*), actin, or lamin. The intensity of each band in three independent experiments (one of them is shown in *A*, *D*, and *F*) was determined and expressed relative to the control (*B*, *E*, and *G*, respectively). Values are the mean ± S.D. ($n = 3$). **, $p < 0.01$; *, $p < 0.05$.

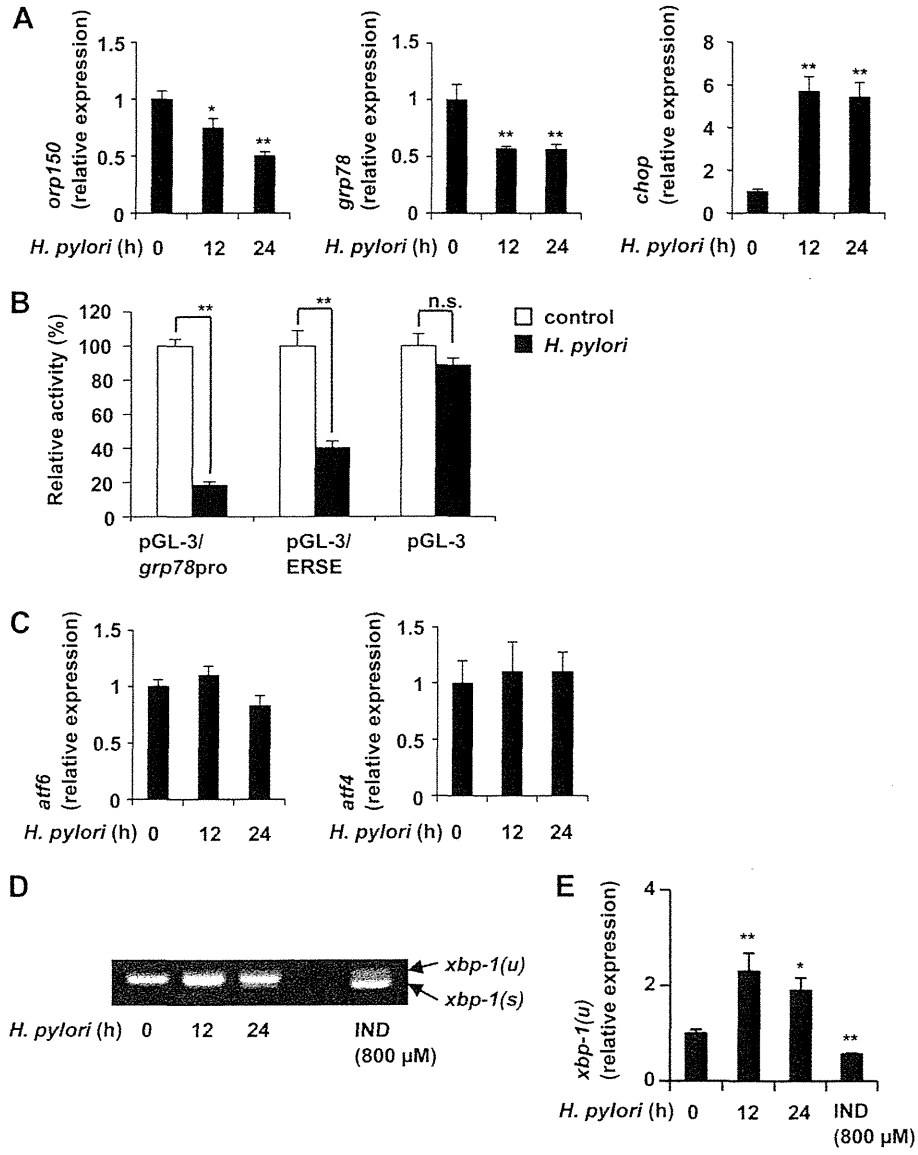

FIGURE 2. **Inhibitory effects of *H. pylori* on transcription of ER stress response-related genes.** AGS cells were co-cultured with *H. pylori* at a bacteria:cell ratio of 200:1 for the indicated periods (*A* and *C–E*) or treated with indomethacin (*IND*) for 24 h (*D* and *E*). *A*, *C*, and *E*, the relative expression of each gene was monitored by real-time RT-PCR using a specific primer for each gene. Values normalized to the *actin* gene are expressed relative to the control sample. *B*, AGS cells were co-transfected with pRL-SV40 (internal control plasmid carrying the *R. reniformis* luciferase gene) and pGL-3 or its derivatives (pGL-3/*grp78*pro and pGL-3/ERSE) and cultured for 24 h. Cells were then co-cultured with or without *H. pylori* at a bacteria: cell ratio of 200:1 for 24 h, and *P. pyralis* luciferase activity was measured and normalized for *R. reniformis* luciferase activity. The 100% value of the *P. pyralis* luciferase activity is 5.4×10^6, 7.4×10^5, or 2.4×10^4 units for pGL-3/*grp78*pro, pGL-3/ERSE, or pGL-3, respectively. *D*, RT-PCR was performed with total RNAs and primer sets for detecting the un-spliced (*xbp-1(u)*) and spliced (*xbp-1(s)*) forms of *xbp-1* mRNA, which were separated by agarose gel electrophoresis. Values are the mean ± S.D. ($n = 3$). **, $p < 0.01$; *, $p < 0.05$; *n.s.*, not significant.

treatment of cells with *H. pylori* cell lysates, but the decrease occurred more slowly than that of ORP150 and GRP78.

As described above, *atf6* mRNA expression was not affected by *H. pylori* (Fig. 2*C*). Thus, either suppression of translation or post-translational modification of ATF6 (such as degradation by proteases) may be responsible for the observed reduction in the level of ATF6 after co-culture of cells with *H. pylori*. To address this issue, we first examined the effect of *H. pylori* on the level of ATF6 in cells pretreated with cycloheximide, an inhibitor of protein synthesis. As shown in Fig. 4*A*, the *H. pylori*-dependent decrease in the level of ATF6 was observed even in cells pretreated with cycloheximide. We also found that the *H. pylori*-dependent decrease in the level of ATF6 was observed for GFP-ATF6, whose expression is regulated by the strong cytomegalovirus promoter (Fig. 4*B*). We also examined the effect of *H. pylori* on the stability of p90-ATF6 by the pulse-chase experiment. As shown in Fig. 4, *C* and *D*, the labeled p90-ATF6 disappeared more rapidly in the presence of *H. pylori* treatment than its absence. These results suggest that post-translational modification of ATF6, such as protein degradation, is responsible for the lower level of ATF6 observed after treatment of cells with *H. pylori*.

In addition to cleavage by S1P and S2P, it is known that ATF6 is continuously degraded by the proteasome-ubiquitin pathway (50, 51). Thus, using specific inhibitors, we examined the contribution of these systems to the *H. pylori*-dependent decrease in the level of ATF6. As shown in Fig. 4*E*, an inhibitor of the proteasome-ubiquitin system, epoxomycin, weakly suppressed the *H. pylori*-dependent decrease in the level of ATF6. On the other hand, an inhibitor of S1P, 4-(2-aminoethyl)-benzenesulfonyl fluoride (AEBSF), did not affect the level of ATF6 in the presence of *H. pylori* (Fig. 4*F*). Furthermore, we found that inhibitors of lysosomal proteases (pepstatin A (an inhibitor of aspartate proteases) and E-64-d (an inhibitor of cysteine protease)) also weakly suppressed the *H. pylori*-dependent decrease in the level of ATF6 (Fig. 4*G*). Interestingly, combination of epoxomycin and inhibitors of lysosomal proteases resulted in clear suppression of the *H. pylori*-dependent decrease in the level of ATF6 (Fig. 4*H*). The results in Fig. 4 suggest that *H. pylori* decreases the level of ATF6 partly through modulation of its degradation by the proteasome-ubiquitin and lysosomal systems.

We also examined the effect of *H. pylori* on subcellular localization of ATF6 using GFP-ATF6. As shown in Fig. 4*I*, GFP-ATF6 co-localized with GRP94 (ER marker). Although the level of GFP-ATF6 was decreased, the localization of ATF6 was not clearly affected by treatment of cells with *H. pylori* (Fig. 4*I*).